ÇUKUROVA UNIVERSITY
INSTITUTE OF NATURAL AND APPLIED SCIENCES

MSc THESIS

Adil Hakan CENGİZ

MODELING OF FAST DC CHARGER FOR ELECTRIC VEHICLES AND INTEGRATION TO GRID

DEPARTMENT OF ELECTRICAL AND ELECTRONICS ENGINEERING

ADANA, 2015

ÇUKUROVA UNIVERSITY
INSTITUTE OF NATURAL AND APPLIED SCIENCES

MODELING OF FAST DC CHARGER FOR ELECTRIC VEHICLES AND INTEGRATION TO GRID

Adil Hakan CENGİZ

MSc THESIS

DEPARTMENT OF ELECTRICAL AND ELECTRONICS ENGINEERING

We certify that the thesis titled above was reviewed and approved for the award of degree of the Master of Science by the board of jury on 27/01/2015.

.....	…….....	.....
Prof. Dr. Mehmet TÜMAY	Asst. Prof. Dr. M. Ugraş CUMA	Asst. Prof. Dr. Lütfü SARIBULUT
SUPERVISOR	MEMBER	MEMBER

This MSc Thesis is written at the Department of Institute of Natural And Applied Sciences of Çukurova University.
Registration Number:

Prof. Dr. Mustafa GÖK
Director
Institute of Natural and Applied Sciences

ABSTRACT

MSc THESIS

MODELING OF FAST DC CHARGER FOR ELECTRIC VEHICLES AND INTEGRATION TO GRID

Adil Hakan CENGİZ

ÇUKUROVA UNIVERSITY
INSTITUTE OF NATURAL AND APPLIED SCIENCES
DEPARTMENT OF ELECTRICAL ELECTRONICS ENGINEERING

Supervisor : Prof. Dr. Mehmet TÜMAY
Year: 2015, Pages: 75
Jury : Prof. Dr. Mehmet TÜMAY
: Asst. Prof. Dr. M. Uğraş CUMA
: Asst. Prof. Dr. Lütfü SARIBULUT

Energy consumption is increasing gradually with worldwide industrialization. The increase in consumption of energy creates a big amount of demand for production which is supplied by fossil fuels. The consumption of fossil fuels leads to environmental pollution. Additionally, limited petroleum reserves are remained.

There is an enormous amount of fossil fuel consumption by internal combustion vehicles that are the most widely used vehicles worldwide. In addition to this, electric vehicles are clean, silent and simple to operate. Because of these reasons, the demand for electric vehicles is increasing.

In this thesis, charger circuit for electric vehicles and its integration to grid are studied. In the study, significant charger modeling topologies in the literature are investigated. Advantages and disadvantages of these topologies are discussed. Among these topologies, one of the most common (constant current-constant voltage) topology is used. The best advantage of the studied topology is recharging the battery in the most appropriate manner. Data of Çukurova University's infrastructure is used for the system. Additionally, in the study we will examine the current drawn by the system, whether the infrastructure is adequate or not. If the results of the examination are found to be inadequate, then we should determine where new infrastructure systems will be needed. Also, the performance of charging station and grid for different cases are analyzed; response of multiple synchronous charging is also investigated.

Key Words: Battery Charge, Charger, Charging Station, Electric Vehicles, Integration to Grid

ÖZ

YÜKSEK LİSANS TEZİ

ELEKTRİKLİ ARAÇLAR İÇİN HIZLI DA ŞARJ EDİCİ MODELİ VE ŞEBEKEYE ENTEGRASYONU

Adil Hakan CENGİZ

ÇUKUROVA ÜNİVERSİTESİ
FEN BİLİMLERİ ENSTİTÜSÜ
ELEKTRİK ELEKTRONİK MÜHENDİSLİĞİ ANABİLİM DALI

Supervisor : Prof. Dr. Mehmet TÜMAY
Year: 2015, Pages: 75
Jury : Prof. Dr. Mehmet TÜMAY
: Yrd. Doç. Dr. M. Uğraş CUMA
: Yrd. Doç. Dr. Lütfü SARIBULUT

Dünya çapındaki endüstriyelleşme enerji tüketiminin giderek artmasına sebep olmuştur. Artan bu tüketim fosil yakıtlar tarafından sağlanmaktadır. Fozil yakıt tüketimi çevre kirliliğine sebep olmaktadır. Buna ek olarak dünya fosil yakıt rezervleri ise az kalmıştır.

Dünya genelinde kullanılan içten yanmalı motorlu araçların yakıtları da fosil yakıtlar olup fosil yakıt tüketiminin büyük çoğunluğunu onlar oluşturmaktadır. Bunun yanı sıra elektrikli araçlar gelenekel araçlara gore temiz, sessiz ve kullanımı daha kolaydır. Bu sebeplerde ötürü elektrikli araçlara olan talep artmıştır.

Bu tez çalışmasında elektrikli araçlar için şarj edici devre modellemesi yapılarak sisteme entegrasyonu çalışılmıştır. Çalışmada aynı zamanda literatürdeki önemli elektrikli araç şarj edici devre modellemeleri incelenmiş, bunların avantaj ve dezavantajları tartışılmıştır. Bu topolojilerden en yaygın olan sabit akım sabit gerilim modeli çalışmaya uygulanmıştır. Bu topolojinin en büyük avantajı bataryayı en uygun şekilde tamamen doldurabilmektir. Daha sonra bu topoloji ile sistem modellenerek değişik durumlardaki davranışlar incelenmiştir. Sistem simülasyonu için Çukurova Üniversitesinin altyapısı kullanılmıştır. Buna ek olarak, elektrikli araç şarj olurken sistemden çekilen akım ve harmonik değerleri, altyapının yeterli olup olmaması gibi konular araştırılmıştır. Araştırmalar sonucunda altyapının yetersiz olduğuna kanaat getirilirse kurulu sistemin nerelerde yetersiz kaldığı tespit edilip yeni altyapı sistemlerinin nerelerde ihtiyaç duyulacağı belirlenecektir. Çalışmada incelenen örnek olaylarda şarj istasyonu ve sistemin performansları analiz edilmiş olup, aynı zamanda birden çok elektrikli aracın şarj edilmesi durumları incelenmiştir.

Anahtar Kelimeler: Batarya Şarjı, Şarj Edici, Şarj İstasyonu, Elektrikli Araç, Şebeke Entegrasyonu

ACKNOWLEDGEMENTS

First and foremost, I offer my sincerest and deepest gratitude to my supervisor, Prof. Dr. Mehmet TÜMAY, who has supported me throughout my thesis with his patience; thanks to him for his trust, guidance and support.

Very sincere thanks are due to Asst. Prof. M. Uğraş CUMA who made every effort to put me on the right track during my MSc study. His constructive notes always resulted in improvements to my work.

I have not enough words to thank my mother, who have been inspiring me and pushing me forward all the way. Their prayers and blessings were no doubt the true reason behind any success I have realized in my life.

The greatest thanks are to Research Asst. M. Mustafa SAVRUN, my colleague and my friend. I have to thank him for his professional and energetic support with helping me during my thesis. Furthermore, his friendship gave me the needed stability in the difficult and demanding phases of this thesis.

Finally, I am grateful to all my family members and friends for their kind support, endurance and encouragements, which have given me the energy to carry on and to motivate myself towards crossing the finish line.

Adil Hakan CENGİZ

CONTENTS **PAGE**

LIST OF TABLES **PAGE**

LIST OF FIGURES **PAGE**

LIST OF SYMBOLS

α	:	Firing Angle
ϕ	:	Phase Angle
θ	:	Conduction Angle
V_{rms}	:	RMS Voltage
i_d	:	Direct Current
i_q	:	Quadrature current
f	:	Fundamental Supply Frequency
i_a	:	Phase A Current
i_b	:	Phase B Current
i_c	:	Phase C Current
I_{load}	:	Load Current
I_{ref}	:	References Current
U	:	Voltage
V_{ref}	:	References Voltage
w	:	Angular Frequency
t	:	Time
V_{ac}	:	Line to Line Voltage A-C
$_{Vbc}$	:	Line to Line Voltage B-C
V_{ab}	:	Line to Line Voltage A-B
V_{an}	:	Line toNeutral Voltage Phase A
V_{bn}	:	Line toNeutral Voltage Phase B
V_{cn}	:	Line toNeutral Voltage Phase C
V_m	:	Sinusoidal Voltage Peak Value
V_{dc}	:	Average Output Voltage
V_{dm}	:	Maximum Average Voltage
V_n	:	Normalized Average Voltage
L_r	:	Reactor Inductance
V_o	:	Output Voltage of Converter
i_r	:	Circulating Current

L_D	:	Converter Inductor
C_D	:	Converter Capacitor
V_D	:	DC Link Capacitor
K	:	Transfer Function Constant
C_{ss}	:	Corresponding Steady State
K_P	:	Proportional Constant
K_i	:	Integral Constant
K_d	:	Derivative Constant
s	:	Laplace Domain Frequency

LIST OF ABBREVIATIONS

AVM	: Average Value Modeling
CC-CV	: Constant Current - Constant Voltage
dq0	: Direct–Quadrature–Zero
EV	: Electric Vehicle
FES	: Flywheel Energy Storage
HF	: High Frequency
ICE	: Internal Combustion Engine
LF	: Low Frequency
HV/LV	: High Voltage / Low Voltage
PFC	: Power Factor Correction Stage
PHEV	: Plug-in Hybrid Electric Vehicles
PID	: Proportional-Integral-Derivative
PLL	: Phase Locked Loop
PWM	: Pulse-Width Modulation
RPM	: Revolutions Per Minute
SC	: Super Capacitor
SOC	: State of Charge
SOE	: State of Energy
THD	: Total Harmonic Distortion
TDD	: Total Demand Distortion
V2G	: Vehicle-to-Grid
0dq	: Zero–Direct–Quadrature
ZEV	: Zero Emission Vehicle

1. INTRODUCTION

Demand for energy is increasing gradually with worldwide industrialization. As well as industrialization, there are plenty of reasons such as population growth, inefficient usage of resources, technological developments, etc. which increase consumption of energy significantly. The increase in consumption of energy creates a big amount of demand for production which is supplied by fossil fuels. Fossil fuel, which are known as petroleum, natural gas and coal, are hydrocarbon-containing fuel. According to the recent data, which are published in mid-2014, there are petroleum reserves 892 billion tons of coal, 186 trillion cubic meters of natural gas, and 1688 billion barrels of crude oil. These numbers seems to be huge at a glance, but taking into account today's level of extraction proved reserves of coal will be exhausted in approximately 110 years, reserves of natural gas will be exhausted in approximately 55 years, reserves of crude oil will be exhausted in approximately 50 years (BP, 2013).

Pollution has long been a concern for the urban areas across the nation. While this originally was of concern only to large metropolitan areas, today almost every city has air pollution concerns. Some agencies have taken upon themselves the stewardship of this predicament. The ill consequences of pollution have given birth to agencies, which governs emissions in world. These agencies have issued several regulations with the goal of reducing emissions. This has forced conventional and new auto manufacturers to invest in technologies that will lead to the production of zero emission vehicles (ZEVs) and the near zero emission vehicles (i.e. hybrid vehicles). With the increasing interest in green technologies in transportation, plug-in hybrid electric vehicles (PHEV) have proven to be the best short-term solution to minimize greenhouse gases emissions (Mehdi et al., 2010). Alternative energy sources are of great importance when running out of fossil fuels and damage caused by them to the nature is considered. Many studies in literature, point to renewable energy resources in order to substantially reduce fossil fuel dependence. Apart from these studies, electric vehicle topic is another work field for reducing fossil fuel dependence. Considering the worldwide number of internal combustion vehicles, an

enormous amount of fossil fuel consumption is concerned. Given that electric vehicles will take internal combustion vehicles places, there will be a remarkable amount of reduction in the usage of fossil fuels. In addition to this, electric vehicles are clean, silent and simple to operate, electric motors has a constant relationship of torque to revolutions per minute (RPM), and features like regenerative breaking, etc. Thus, electric vehicles have more advantages when they are compared with internal combustion vehicles.

Today, the demand for electric vehicles is increasing. Manufacturers have focused their research and development activities on the electric vehicles. The number of electric vehicles on the market is increasing day by the day. Therefore, the electric vehicle infrastructure technologies are also being developed. Some of the technology infrastructures are as follows: battery systems, communications, network integration, charging systems.

As a result, the purpose of this study is examining electric vehicle infrastructure technology in the charging systems and network integration issues. Battery charging systems and charging stations that are one of the important building blocks of electric vehicles' simulation, which will be applied in the university, is studied. In this study we will examine the current drawn by the system when electric vehicle is charging, whether the infrastructure is adequate or not, where we should need new infrastructure systems when installed infrastructure is not sufficient, etc.

1.1. Outline of Dissertation

In Chapter 2, previous studies are mentioned about charging systems and grid integration which are studied by different researchers. Furthermore, similar models are searched for comparison with available studies in the literature.

In Chapter 3, control methods are described in detail. Pulse-Width Modulation (PWM) method that is used in charging system is examined.

In Chapter 4, charging circuit configuration, controller circuit configuration and parameters of system and battery are given and evaluated.

In Chapter 5, simulation results for different case studies are given and evaluated. In these cases, the performance of charging station and grid for different cases are analyzed; response of multiple vehicles' charging is also investigated.

In Chapter 6, the important conclusions of the study and author's recommendations for future work are explained.

Finally, related references used in the thesis and biographical information of the author are presented.

2. LITERATURE REVIEW

2.1. Introduction

A lot of studies have been made and are available in the literature about charging stations and grid integration. Also, the subject of battery charging has its own sub-topics e.g. current control, voltage control in some studies. Additionally, it is known that control of charging current and charging voltage are important factors for the battery charging in electric vehicles. Therefore, these studies are also detailed in the literature review. Commonly, numerical and experimental studies are made.

Yilmaz and Krein (2013) examined battery charger topologies, charging power levels and infrastructure for plug-in electric and hybrid vehicles in the literature. They are categorized the charger systems as off-board and on-board types with unidirectional or bidirectional power flow. They emphasized the limitations and advantages of the battery charger types as unidirectional charging limits hardware requirements and simplify interconnection issues, bidirectional charging supports battery energy injection back to the grid, on-board charger restrain power because of weight, space and cost constrains, an off-board charger can be designed for high charging rates and is less constrained by size and weight. In the paper, various power level chargers and infrastructure configurations are presented, compared, and evaluated based on amount of power, charging time and location, cost, equipment, and other factors. Topologies indicated in the paper are as follows; as can be seen from Figure 2.1, it consists of two boost converters in parallel operating 180^{o} out of phase. The interleaved boost converter has the advantage of paralleled semiconductors. With ripple cancellation at the output, it also reduces stress on output capacitors. Another charging topology is presented in Figure 2.2. The topology of a single-phase unidirectional multilevel charger is suitable, and is a common multilevel charger topology for low-power level charging. Three-phase bidirectional multilevel converters are recommended for high-power level charger systems.

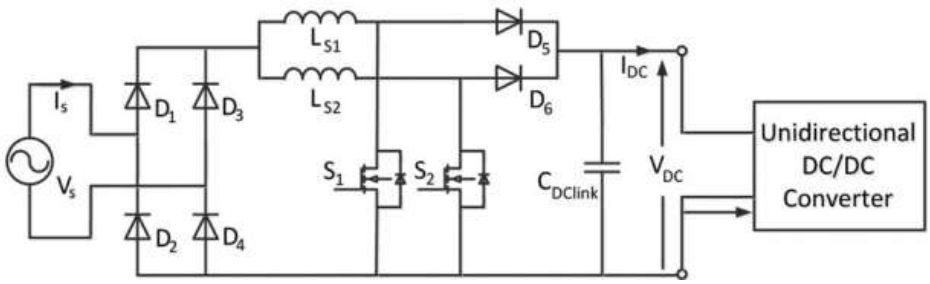

Figure 2.1. Interleaved unidirectional charger topology (Yilmaz and Krein, 2013)

A further topology is three-level bidirectional dc-dc converters. Thus, it has been investigated for charge station application as others by author as shown in Figure 2.3. These converters are characterized by low switch voltage stress and used in smaller energy-storage devices such as indicator and capacitors.

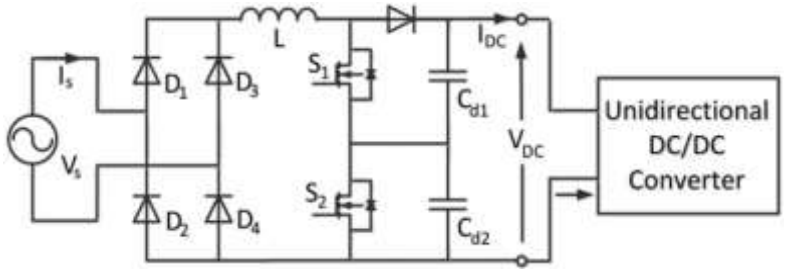

Figure 2.2. Single-phase unidirectional multilevel charger circuit (Yilmaz and Krein, 2013)

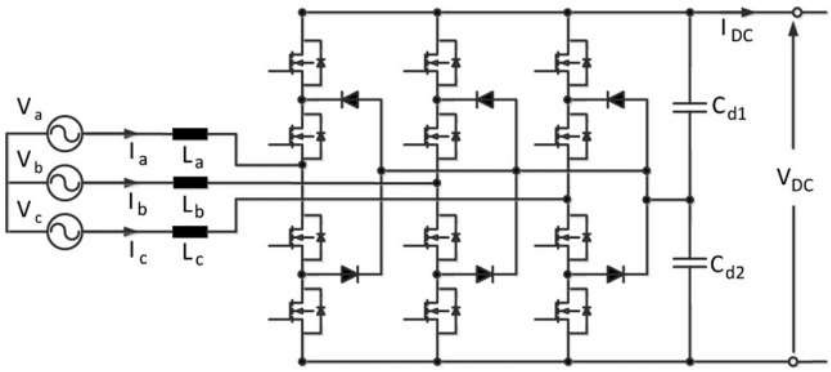

Figure 2.3. Three-level diode-clamped bidirectional charger circuit (Yilmaz and Krein, 2013)

There are various topologies and schemes reported in literature for both single-phase and three-phase chargers. These chargers are using half bridge or full

bridge rectifier topologies. The difference between each other can be summarized by author as the half-bridge has fewer components and lower cost, but exhibits high component stress and full-bridge systems have more components and higher cost, with lower component stress. This topology that is mentioned in Figure 2.4 requires more pulse-width modulation inputs that add to the complexity and cost of the circuitry. Figure 2.4(a)–(c) shows basic bidirectional circuits. Figure 2.4(a) shows a single-phase half-bridge bidirectional charger. Figure 2.4(b) shows a single-phase full-bridge charger, and Figure 2.4(c) shows a three-phase full-bridge bidirectional unit that interfaces to a dc–dc converter.

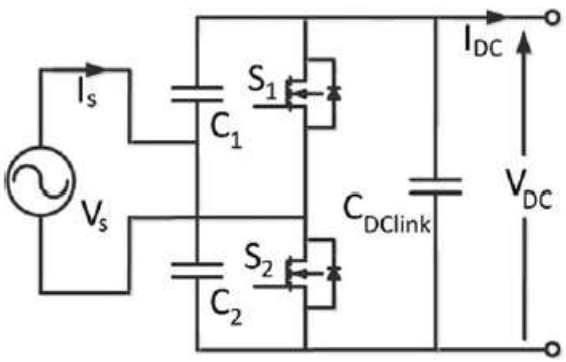

(a)

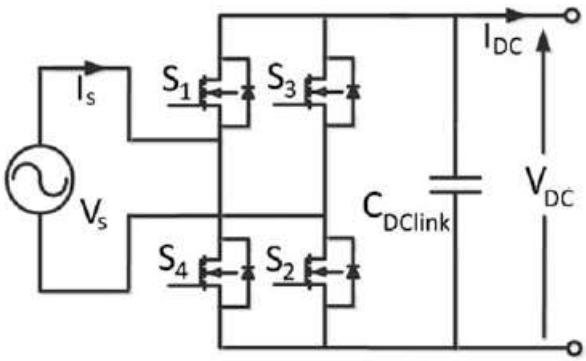

(b)

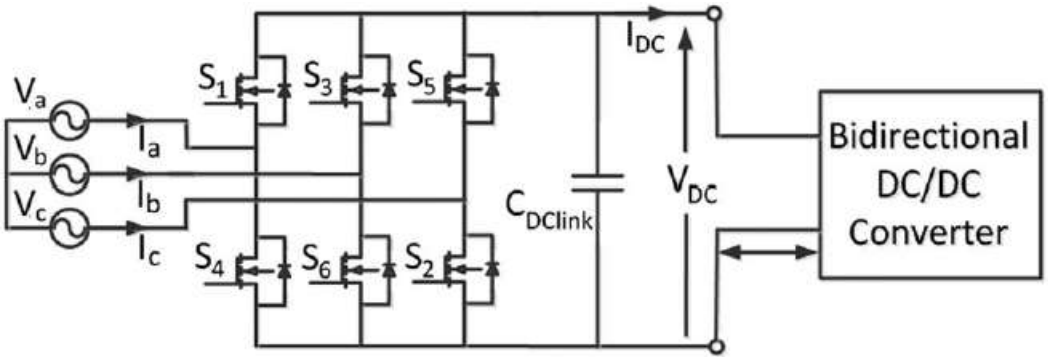

(c)

Figure 2.4. Bidirectional chargers: (a) single-phase half-bridge, (b) single-phase full-bridge, and (c) three-phase full-bridge (Yilmaz and Krein, 2013)

Erb et al. (2010) investigated the bi-directional charging topologies for plug-in hybrid electric vehicles. Firstly, they reviewed some of the power electronic topologies of bi-directional AC-DC and DC-DC converters, than they selected the best choice for combining two topologies to form a bi-directional charger. As can be seen from Figure 2.5, primarily, general charger structure is presented in the paper. Furthermore, there are three topologies mentioned under bi-directional AC-DC converters heading and there are also three topologies mentioned under bi-directional DC-DC converters heading in the study. These topologies are Half-Bridge PWM AC-DC Converter, Full-Bridge PWM AC-DC Converter, Three-Level PWM AC-DC Converter, Dual Active Bridge DC-DC Converter, Two Quadrant DC-DC (Buck-Boost) Converter and Integrated Buck-Boost DC-DC Converter respectively.

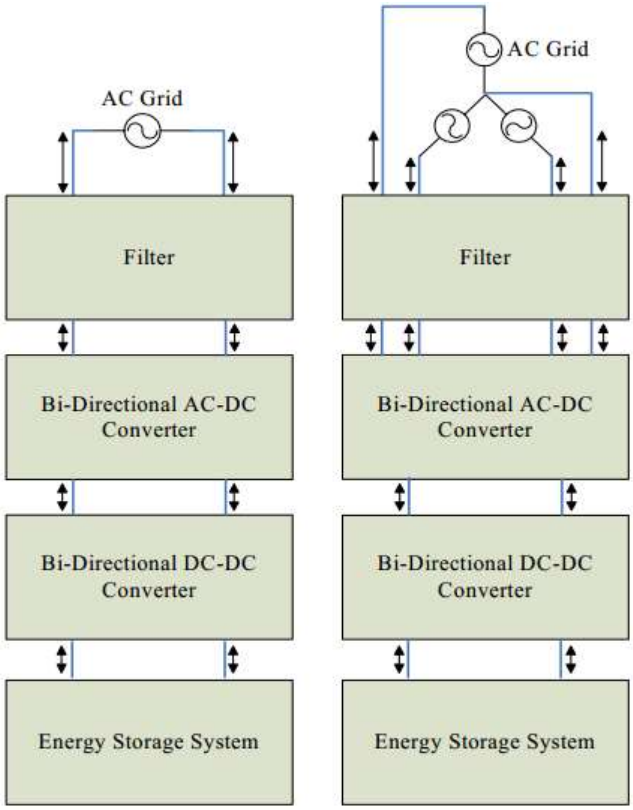

Figure 2.5. General bi-directional charger topology for single-phase (left) and three-phase systems (right) (Erb et al., 2010)

Dubey et al. (2013) studied average value model of electric vehicle chargers. The model that is proposed in the paper is developed based on the average value modeling (AVM) approach. Their circuit structure includes a rectifier circuit along with PWM control, boost converter and battery banks. Average dynamics of the switching circuit are obtained by averaging the effects of fast switching in the device that occur within a prototypical switching interval. The proposed AVM is validated against a switching model and the actual measurements taken at an EV charging facility and is found to be very accurate in approximating EV charger behavior. The electric vehicle (EV) battery charger block diagram shown in Figure 2.6 consists of three stages as the first stage consists of an input filter and a full-bridge rectifier to convert AC power to DC power. The second stage is a boost converter with a power factor correction stage (PFC) to condition the input current as a sinusoidal waveform. The boost converter is required to step-up input voltage to a level compatible with the electric vehicle battery voltage. The third stage isolates the battery from the

supply power system. It is comprised of a full-bridge forward (DC-DC) converter with a low-pass filter connected to its output terminals. The detailed circuit diagram is shown in Figure 2.7.

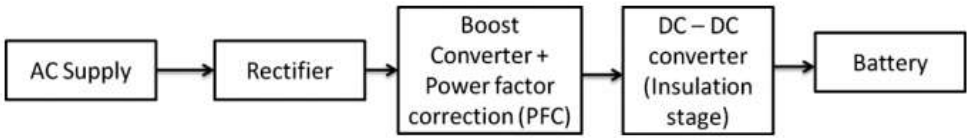

Figure 2.6. Block diagram of an EV battery charger (Dubey et al., 2013)

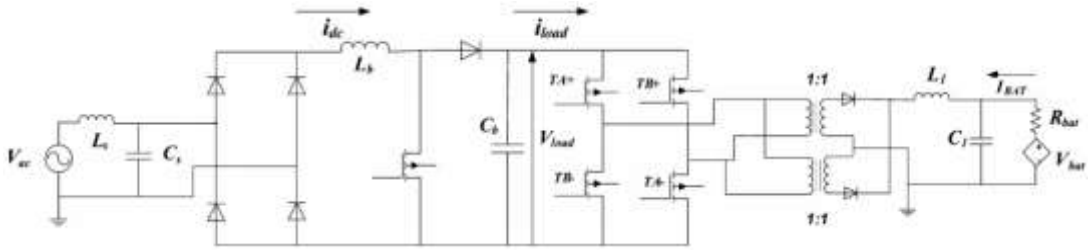

Figure 2.7. EV battery charger with PWM control circuit diagram (Dubey et al., 2013)

The full-bridge DC-DC converter associated with the insulation stage is controlled using the PWM technique, the block diagram for which is shown in Figure 2.8. The PWM scheme controls all four switches using bi-polar voltage switching. The proposed method is tested in different cases in a simulation study in the paper.

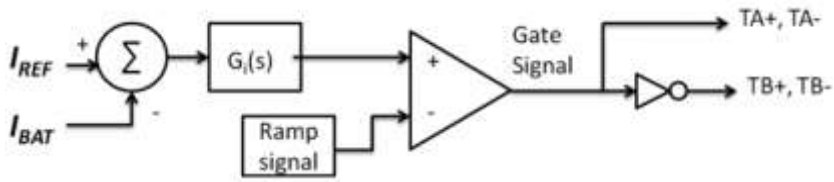

Figure 2.8. Block diagram of PWM control of DC-DC converter (Dubey et al., 2013)

Veneri et al. (2013) investigated performance analysis on power architecture for EV ultra-fast charging stations. They focus on the design criteria of the power conversion systems operating within ultra-fast charging stations for electric vehicles. Their proposed architecture is based on a DC bus (in Figure 2.9), which features the integration of renewable energy sources and buffered storage systems, performing the new concept of smart grid system. The proposed architecture presents the

advantage of the AC/DC grid tie converter conveniently and efficiently downsized with respect to the actual power needed to recharge the electric vehicles. Firstly, they described EV charging architectures drawing particularly attention to the main issues of ultra-fast charging, and a DC buffer charging architecture is proposed as a case study.

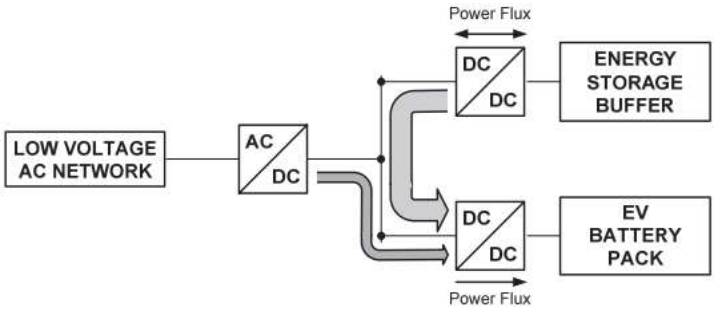

Figure 2.9. EV Charging architecture with energy storage buffer (Veneri et al., 2013)

Arancibia and Strunz (2012) examined electric vehicle charging station for fast DC charging. Their proposed model of an electric vehicle charging station is suitable for the fast charging of multiple electric vehicles. The station consists of a single grid-connected inverter with a DC bus where the electric vehicles are connected. The control of the individual electric vehicle charging processes is decentralized, while a separate central control deals with the power transfer from the AC grid to the DC bus. Their proposed DC charging station configuration is shown in Figure 2.10, it can be seen that the inverter is interfaced to the network through an LCL filter and a transformer; while a single DC bus feeds all individuals battery chargers.

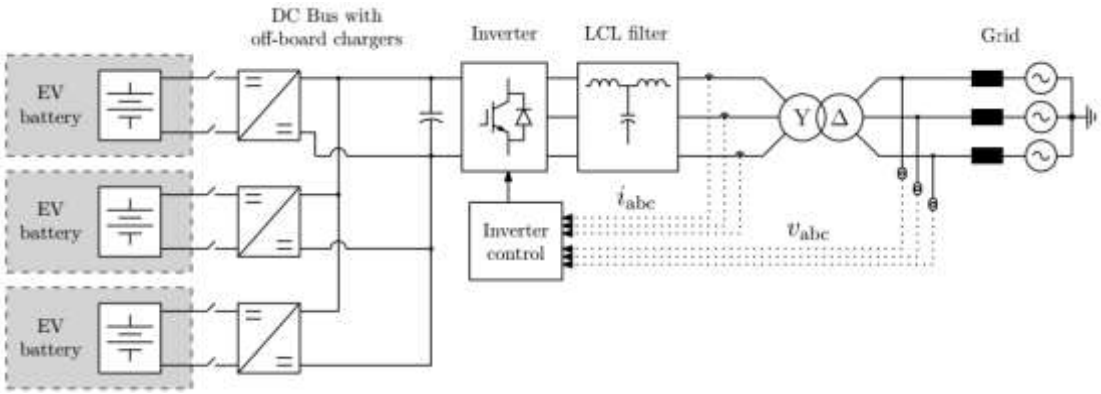

Figure 2.10. Proposed EV charging station for fast DC charging (Arancibia and Strunz, 2012)

In control section of the proposed charging station, a cascade control in the dq-frame is proposed. It consists of outer voltage loop and inner current loop. Synchronization with the grid voltage is performed through a phase locked loop (PLL). The proposed control methodology is depicted in Figure 2.11.

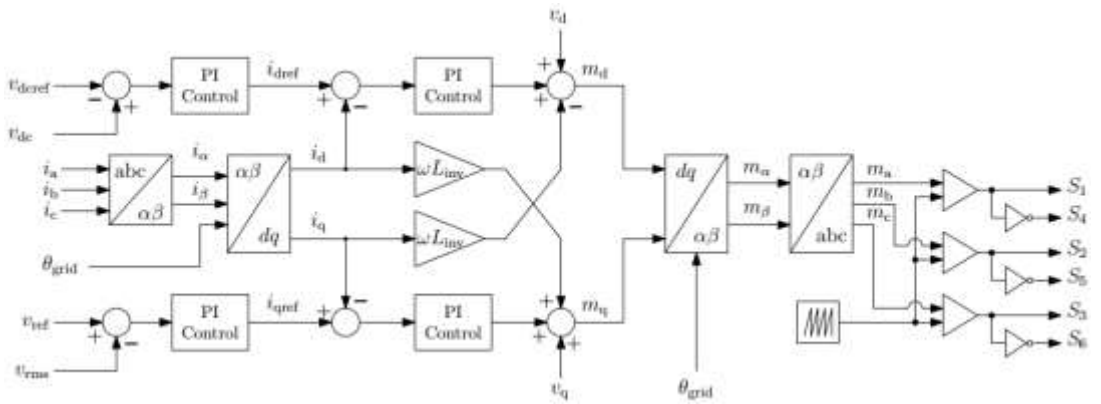

Figure 2.11. Charging station control system (Arancibia and Strunz, 2012)

Kisacikoglu et al. (2013) examined EV/PHEV bidirectional charger assessment for vehicle-to-grid (V2G) reactive power operations in the literature. In this study, single phase ac-dc topologies used for EV/PHEV, level-1 and level-2 on-board charging topics are presented. Classification of the chargers based on their vehicle-to-grid usage is given and design criterias of single-phase on-board chargers are described in detail. Furthermore this study adverted on the integration of the grid connected vehicles to the utility grid by explaining PEV chargers, charging terms and definitions, and charger topology selections based on different operation modes.

Topologies indicated in the paper are mainly grouped under two headings, Power Factor Corrected (PFC) Unidirectional Chargers and Four-Quadrant Bidirectional Chargers. PFC Unidirectional Chargers are conventional ac-dc boost converter, interleaved ac-dc boost converter, symmetrical and asymmetrical bridgeless boost rectifiers. Four-Quadrant Bidirectional Chargers are dual-buck ac-dc half-bridge converter, ac-dc half-bridge converter, ac-dc full-bridge converter. In conventional ac-dc boost converter topology, a front-end diode bridge is used to rectify the input voltage, and it is followed by a boost section as shown in Figure 2.12. This topology is widespread for low-power applications. Due to conduction losses of the diode bridge, it is not well suited for power levels higher than 1 kW Musavi et al. (2011), Figueiredo et al. (2010).

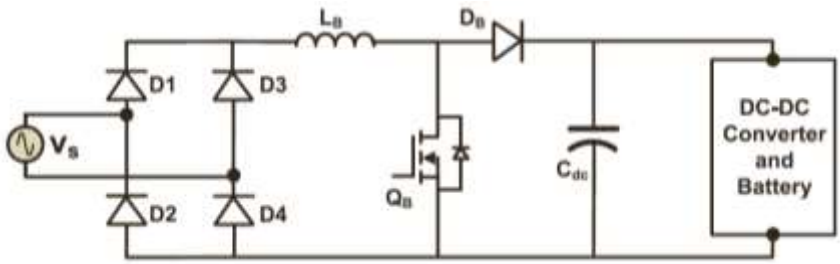

Figure 2.12. Conventional AC-DC boost converter (Kisacikoglu et al., 2013)

In interleaved ac-dc boost converter topology shown in Figure 2.13, the main advantage is decreased high-frequency pulse width modulation (PWM) rectifier input current ripple caused by the switching action. Reducing input ripple decreases the required switching frequency to meet a current total demand distortion (TDD) limit imposed by the utility.

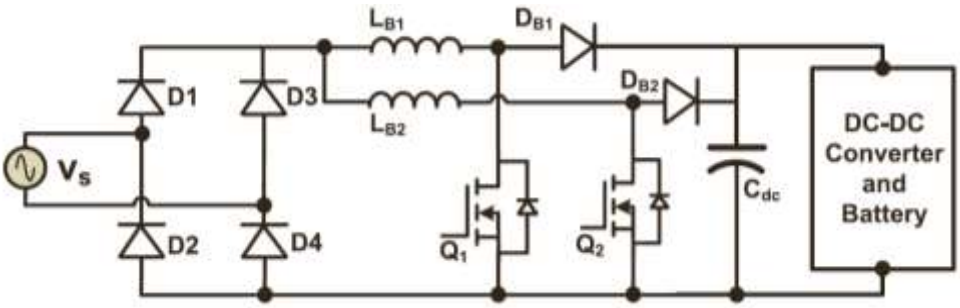

Figure 2.13. Interleaved AC-DC boost converter (Kisacikoglu et al., 2013)

Another advantage is the reduced current rating of the active switches as the interleaving converter halves the input current. One disadvantage of the topology is the high conduction losses of the input bridge rectifier as well as increased number of semiconductor devices and associated gate control circuitry. This topology is preferred by the industry for on-board charging applications and is used for 3.3-kW level-2 chargers Gautam et al. (2011), Gautam et al. (2012). Symmetrical and Asymmetrical AC–DC Boost Converters topologies are proposed in Martinez and Enjeti (1996) and Lim and Kwon (1999), shown in Figure 2.14 and Figure 2.15 respectively.

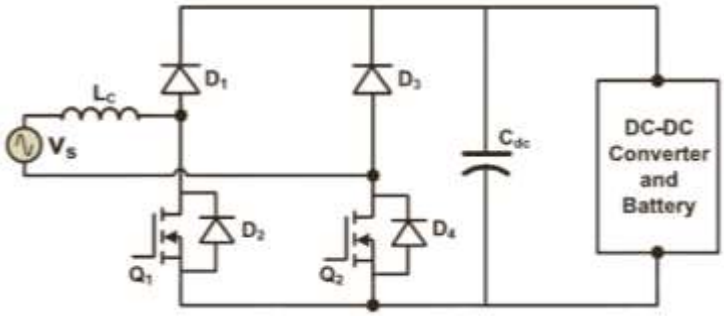

Figure 2.14. Symmetrical bridgeless boost rectifier (Kisacikoglu et al., 2013)

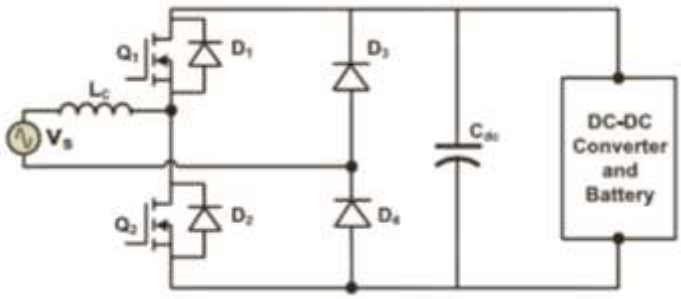

Figure 2.15. Asymmetrical bridgeless boost rectifier (Kisacikoglu et al., 2013)

Advantages of both of these topologies are eliminate the input diode bridge to attain higher efficiencies at increased power levels.

Dual-Buck AC–DC Half-Bridge Converter topology shown in Figure 2.16 and introduced in Stanley and Bradshaw (1999). Also employed for a battery storage system to demonstrate four-quadrant operation capability with increased efficiency.

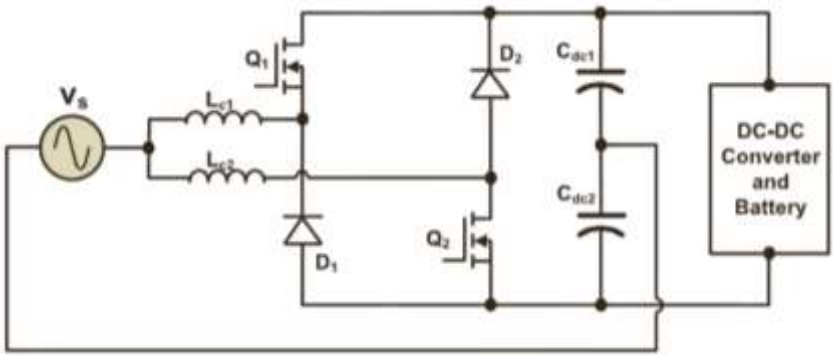

Figure 2.16. Dual-buck- ac-dc half-bridge converter (Kisacikoglu et al., 2013)

The circuit does not need shoot through protection as there are no active switches connected in series. Conventional AC–DC Half-Bridge Converter topology illustrated in Figure 2.17 is suitable to transfer power in four quadrants Qian (2011).

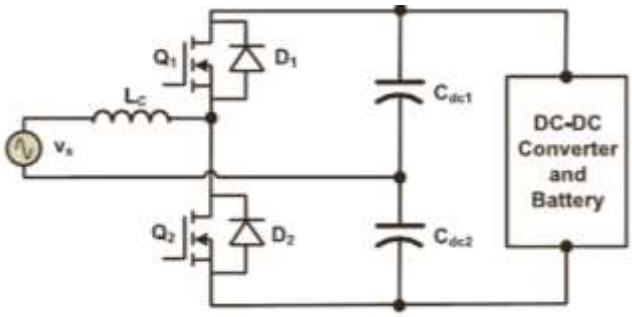

Figure 2.17. AC-DC half-bridge converter diagram (Kisacikoglu et al., 2013)

A half-bridge converter requires bipolar switching because there are only two possible output voltage levels, $+V_{dc}$ and $-V_{dc}$. AC–DC Full-Bridge Converter topology shown in Figure 2.18, is comprised of a dc-link capacitor, four transistors (either MOSFETs or IGBTs), four diodes, and a coupling inductor. Since there are three output voltage levels ($+V_{dc}$,$-V_{dc}$, and zero) for the full bridge inverter, the number of switchings required for the same current THD level is effectively reduced with the full-bridge converter compared to half-bridge converter.

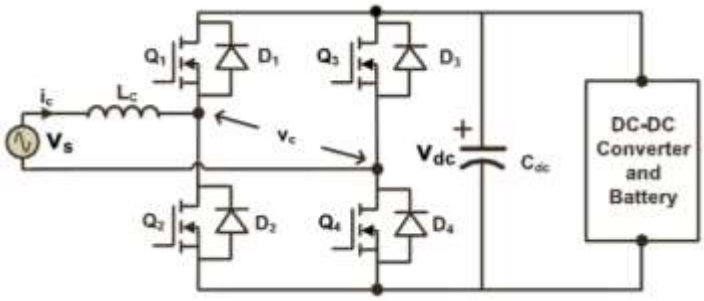

Figure 2.18. AC-DC full-bridge converter diagram (Kisacikoglu et al., 2013)

Mapelli et al. (2013), studied electric bus with fast charging energy storage system based on lithium battery and super capacitors. In this study it is aimed that electrical bus will stop and recharge its super capacitor at each bus stop, for this the energy storage system needs to provide high peak of power and low amount of energy. Taking into account of worst operating condition a conventional battery is installed to the system. The paper deals with the energetic analysis of an electric bus with an hybrid energy storage system composed by batteries and super capacitor. At first the numerical simulation model of each component has given and then the algorithm to split the power demand of the traction drive on the two on board energy storage system is mentioned. This algorithm has been designed in order to let the battery to work as most as possible in a steady state condition. In this way it is possible to extend the battery life because it is discharged in large time periods and without sudden changes in the supplied current. Urban electric bus powertrain analyzed in this paper schematically represented as in Figure 2.19. In this figure it has also be represented the general structure of the charging station at bus stop. Figure 2.20 shows the general structure of the numerical simulation model which has developed using the object oriented approach.

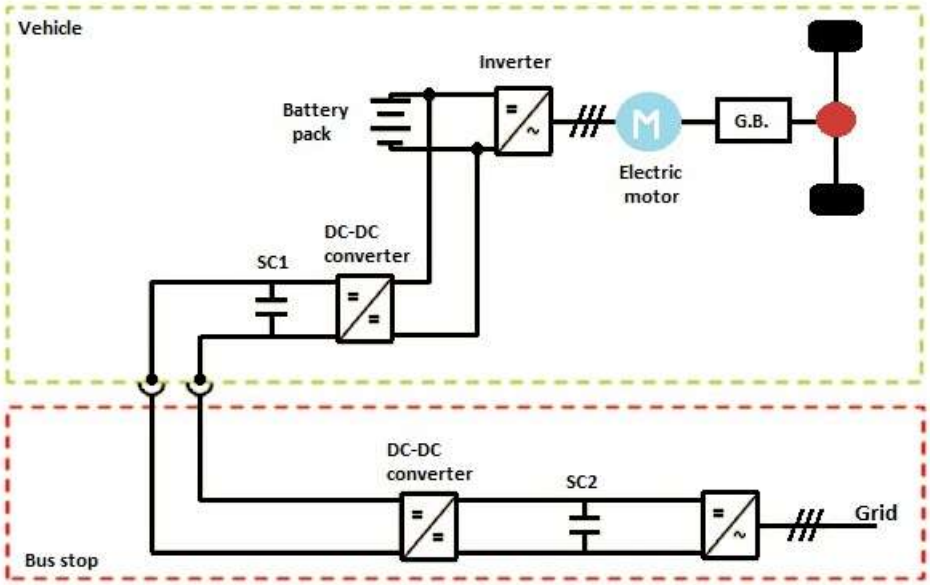

Figure 2.19. Scheme of electric bus power-train and storage system (Mapelli et al., 2013)

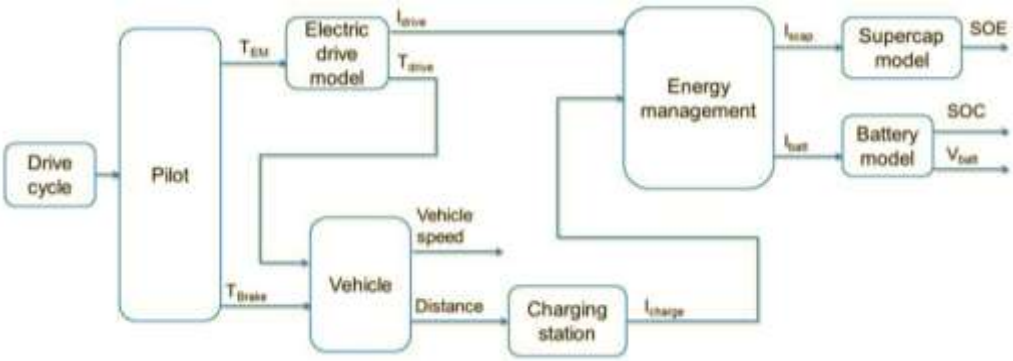

Figure 2.20. General scheme of the simulation model (Mapelli et al., 2013)

In this paper, energy management control algorithm is substantially defined according to the on board energy status: four working areas have been identified limited by various levels of the state of energy (SOE) of the super capacitors as shown in Figure 2.21.

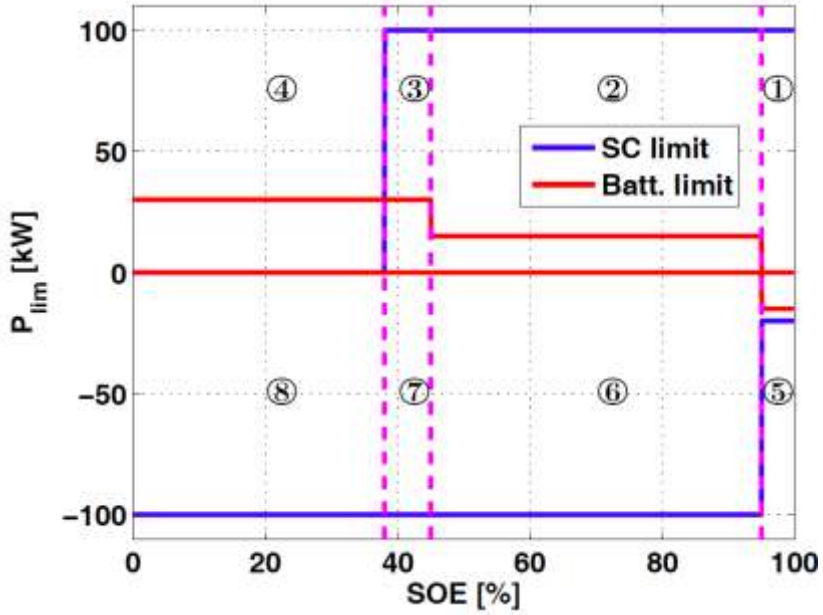

Figure 2.21. Super capacitor and battery limit (Mapelli et al., 2013)

In the portion 1 of the Figure 2.21, where the SOE is over the 95%, the battery is completely turned off and all the inverter power is supplied from the super capacitors. In the portion 2 of the Figure 2.21, where the SOE is between the 45% and 95% the bus is moved with the energy coming both from super capacitors and from the battery. In the part 3 of the Figure 2.21, the SOE is between the 38% and 45% the bus is still moved with the energy of super capacitors and the battery supply the maximum power because the super capacitors are near to their minimum SOE value. Part 4 of the Figure 2.21, the super capacitors are switched off and the energy to move the bus is given only by the battery. At last for the bus braking phases the energy is stored in the super capacitors when the SOE is under 95%, part 6, 7 and 8 of the Figure 2.21, if the SOE is over 95%, part 5, the kinetic energy recovered by the traction drive is stored in the battery.

Tu et al. (2011) examined a research on vehicle-to-grid technology. In this paper, a review of the concept, the functions, the scheme and the economic and social values of vehicle-to-grid (V2G) are discussed. Main focus of this article is to strengthen the regulation and operation management for electric vehicles. Therefore, this paper explains potential values of V2G base on the developmental scale of 2020's electric vehicle in Shanghai.

Even though electricity is grouped in several different markets with correspondingly different control regimes, in this paper only base load power, peak power, spinning reserves, and regulation topics have taken place. However, it is not realistic for electric vehicles to afford base load power because the cost per kWh of electric energy is high and the operation time is limited. On the other hand the economic value of other three services is high and can compensate some of the high initial invest. The combination of spinning reserves and regulation reserves is called "ancillary service". In conclusion, this paper reviews the basic contents of V2G and its influence to the power system.

Freige et al. (2011) investigated power and energy ratings optimization in a fast-charging station for PHEV batteries. This paper justifies the selected power and energy ratings of the respective charging station resources in order to charge the PHEV battery with a maximum capacity of 15 kWh from 20% to 95% of its state-of-charge in a maximum duration of 15 minutes. Configuration of charging station is given in Figure 2.22. The methodology, results and its application are presented. This paper considers a charging algorithm shown in Figure 2.23.

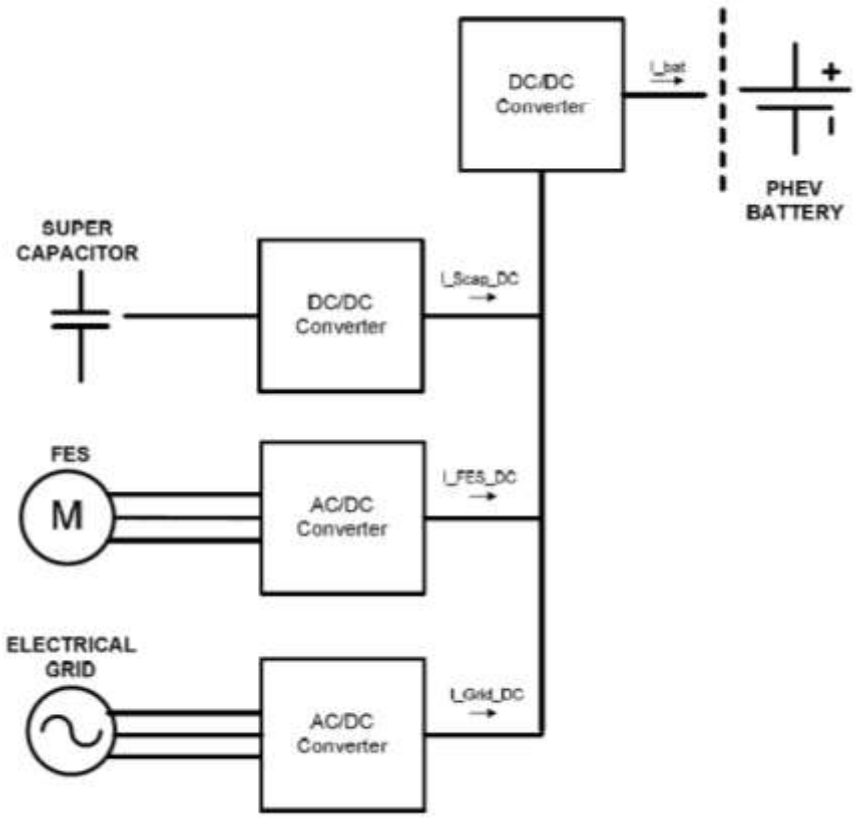

Figure 2.22. Charging station configuration (Freige et al., 2011)

The blue lines for each axis show the power flow for each element of the charger, the grid, and the PHEV battery. Positive power represents that the element is providing or discharging energy, whereas negative power represents that the units are charging.

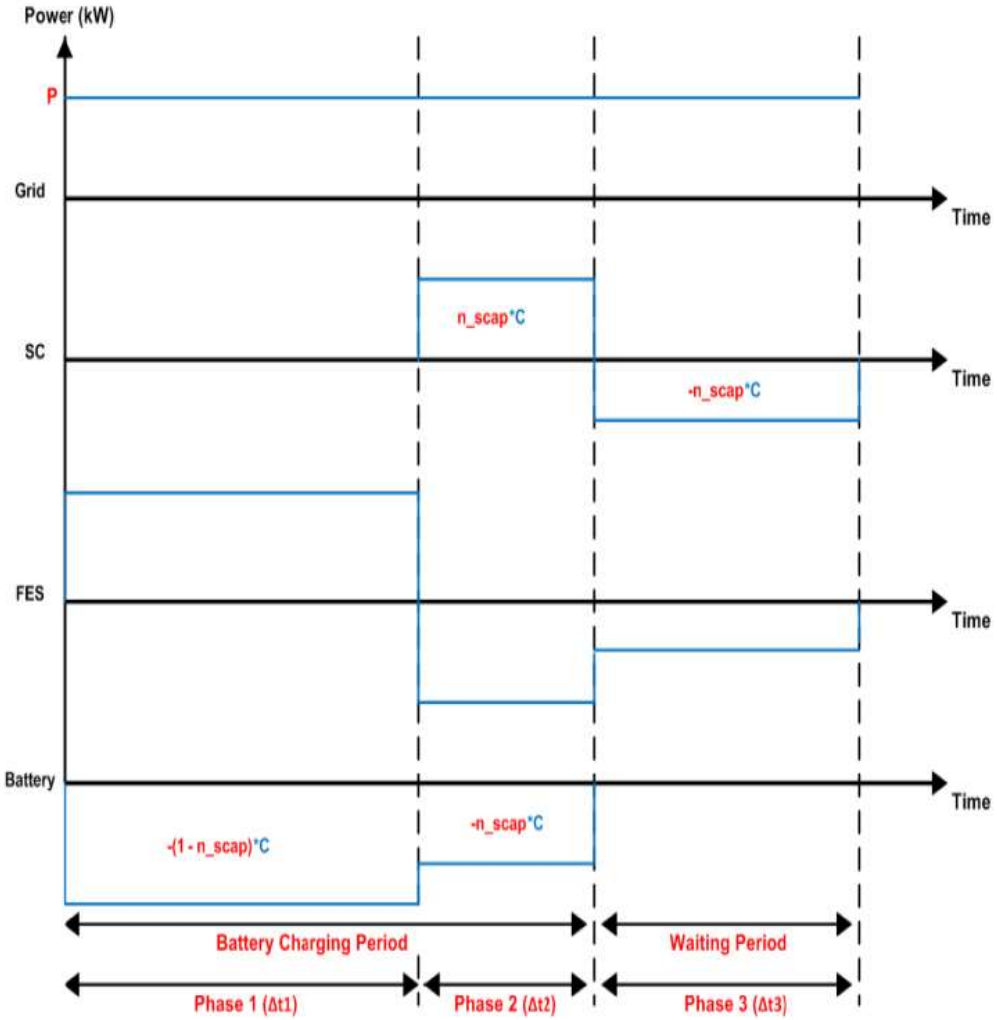

Figure 2.23. Detailed charging station operation, divided into three phases (Freige et al., 2011)

In Phase 1, the Flywheel Energy Storage (FES) and the electrical grid provide energy to the PHEV battery. The super capacitor (SC) remains dormant in this phase. In Phase 2, while the SC provides energy to the PHEV battery until its required capacity, the electrical grid recharges the FES. In Phase 3, the electrical grid recharges the SC and the FES to their respective full capacities. It is also called the "waiting period" because during this time, no PHEV battery is allowed to be connected to the charging station. After this phase is completed, the charging station is ready to charge another PHEV battery, which will restart from Phase 1. Results of the study are summarized in Table 1.

Table 2.1. Grid and ESD parameters (Freige et al., 2011)

	Grid	**FES**	**SC**
Maximum Duration of Operation (min)	10	10	5
Maximum Power (kW)	30	30.75	13.5
Maximum Energy (kWh)	5	5.125	1.125

In conclusion, finding the power and energy ratings of a fast-charging station for PHEV batteries is successful, in addition to the grid, one or more stationary energy storage devices. The power drawn from the grid is minimized, the battery charging process does not exceed 15 minutes, and the replenishment of the storage devices takes no longer than 7.5 minutes. These charging and full-cycle times of the charging station conform to the Level III fast-charger standard, as outlined in the SAE J1772 standard.

In study of Chen et. al. (2012), dynamic simulation of electric vehicle fast charging is inspected using different scenarios. This simulation includes renewable generation, as well. Advantages of coordinated controls of fast charging and renewable generation are highlighted. These advantages are considered from two points of views: grid connection and islanding condition. According to the simulation results, charging stations may have positive effect on reducing the impact of renewable generation fluctuation on voltage sustainability and system frequency. The quantitative results indicate that frequency variation may be reduced by 50% in amplitude. With the developed control strategy (Figure 2.24), they achieved to both reduce the voltage variation during renewable generation fluctuation period and expedite the oscillation damping after the recovery of renewable generation.

Aggeler et. al. (2010), present two converter architectures to be used for fast battery charging applications. Their study is based on both low (LF) and high frequency (HF) isolation requirements. The LF conversion architecture (Figure 2.25) consists of four major parts. One, a 1:1 line-frequency transformer for isolation of the system from the main line. Two, an input LCL filter in order to achieve compatibility to IEC standards. Three, a three phase active rectifier to make sure an active power factor control. Four, a three phase interleaved buck converter to make the battery current controls possible.

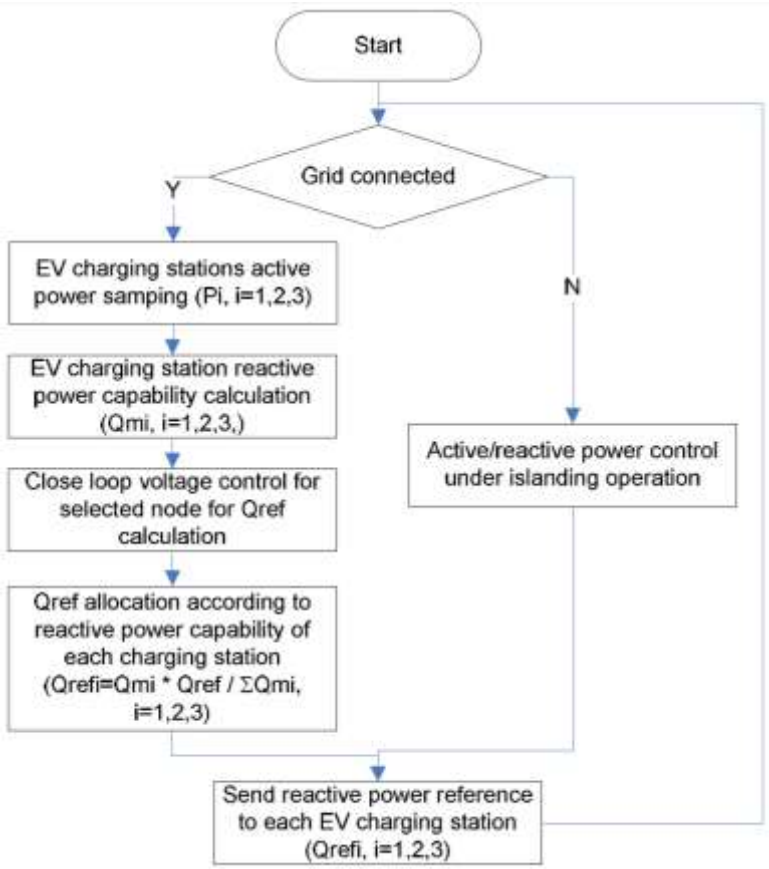

Figure 2.24. Control strategy flow chart for grid-connected scenario (Chen et al., 2012)

On the other hand, the HF conversion architecture (Figure 2.26) consists of three major parts. One, an input LCL filter in order to achieve compatibility to IEC standards. Two, a three phase active rectifier to make sure an active power factor control. Three, two in parallel DC/DC converter stages, for high frequency isolation purpose. The results obtained with the simulation constructed considering the worst case scenario, it is concluded that the voltage variations may be expected between 3%-8% on buses on the vicinity of the charging station.

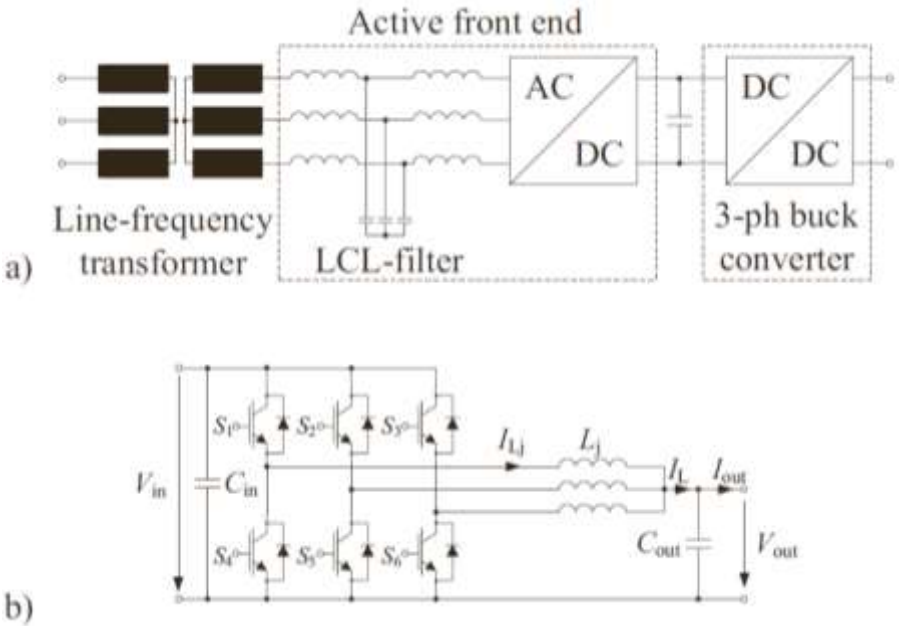

Figure 2.25. (a) LF converter solution for dc fast charging stations and (b) the three phase interleaved buck converter based on the standard ABB product (Aggeler et al., 2010)

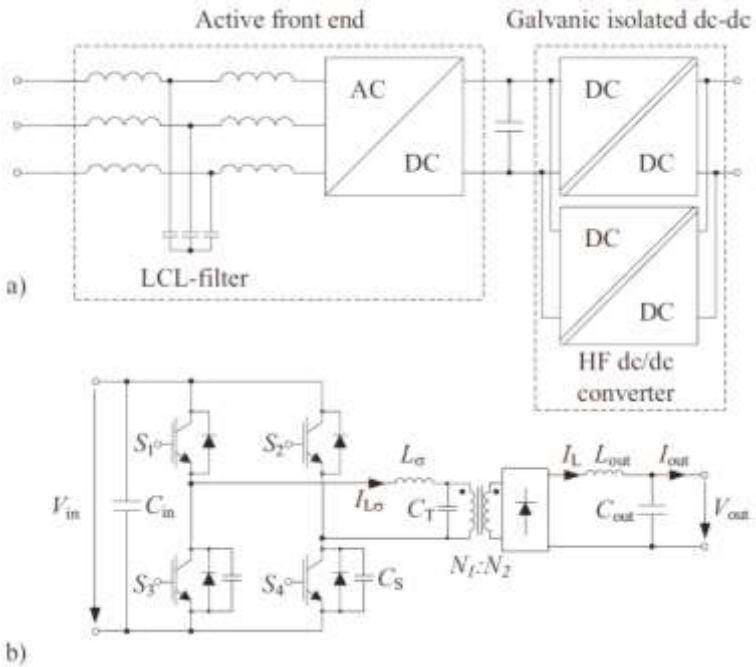

Figure 2.26. (a) HF converter solution for dc fast charging stations with two in parallel connected galvanic isolated dc-dc stages and (b) the corresponding HF dc-dc isolated converter topology (Aggeler et al., 2010)

Kuperman et. al. (2012), presents the functionality of a fast charger for a lithium-ion electric vehicle propulsion battery. The charger is designed as a dual stage controlled ac/dc converter and it is also capable of operating in either constant current, constant voltage or constant power charging mode (Figure 2.27). According to the experiments under 35kW and 50kW charging powers, it is possible to observe that input current is nearly sinusoidal and in phase with mains voltage, the power factor is close to unity and the efficiency is above 95%.

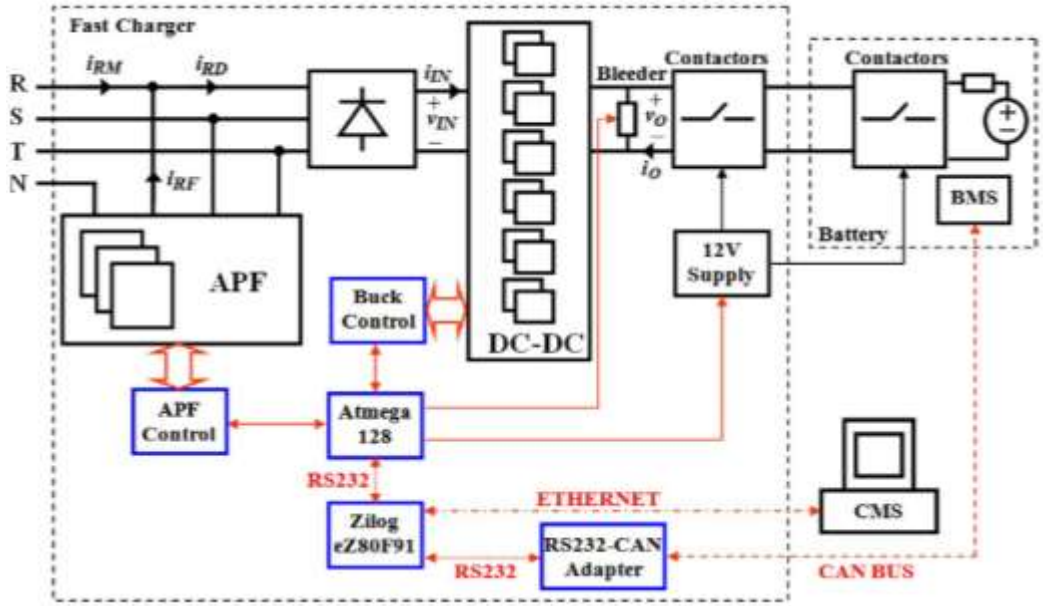

Figure 2.27. Fast-charge system-level block diagram (Kuperman et al., 2012)

Concerning fast charge infrastructure and mobility, two model designs are proposed by Machiels et. al. (2013) based on current mobility behavior in Flanders, first design determines the charging demand. In order to meet the resulting fast charge demand, a charge infrastructure is simulated by the second design. The energy management is handled by such an algorithm that controls the power flows between the photovoltaic installation, grid connection, energy storage system, and the fast chargers. According to the simulation results, it is concluded that using the proposed designs, 99.7% of the vehicles visiting the fast charge station may begin charging within 10 minutes with a configuration limited to 5 charging spots.

Pillai et. al. (2012), examined a case study of EVs in residential areas, in Denmark. In this paper is mainly interested in the local grid limitations to accommodate large amount of EVs of sizable power ratings in residential areas. A detailed low voltage residential distribution grid in Denmark, which modeled in DIgSILENT Power Factory program, is covered as a case study. The electric vehicles are modeled as constant power loads of 11kW capacity in the grid model which are connected to the individual household circuit (three phase, 16A). Some of EV integration scenarios are analyzed for understanding the network operational flexibility and ruggedness. Simulation cases are studied to identify the weak nodes, flexibility in the network and possible strategy to overcome these shortcomings to incorporate more electric vehicles. The simulation results show that level of EV integration varies with the strength of different feeders in the studied network. Simple grid reinforcement measures like adding new feeders in the existing network improves EV penetration levels. The secondary distribution transformer used in this study is characterized by low annual capacity utilization (approx. 15%). This provides sufficient head-space on the transformer capacity to add electric vehicles of ample ratings. These along with storage capabilities of EVs are an ideal situation to support high wind penetration planned in countries like Denmark. Static power system simulation cases are performed in this article to identify major grid bottlenecks to the smooth integration of electric vehicles. The primary constraints include the voltage limits, thermal loading of the cables and feeder characteristics of the secondary distribution grid.

2.2. Conclusion of Literature Review

Several studies are carried out on about battery charging, charging stations and integration of electric vehicles in the literature. Some of them used experimental techniques and the others used simulation analyses. These studies mainly focused on the charging techniques, control topologies and impacts on grid. Also different charging topologies to obtain the best control optimization were searched.

When the studies investigated, although there are many control circuits, it is obviously seen that the charging methods are limited. These charging methods are constant current, constant voltage, etc. On the other hand, grid penetration studies mainly include percentage penetration levels until the examined grid can't support EV charging any more.

In this thesis, constant current - constant voltage (CC-CV) method is used as battery charging topology. Additionally, in case studies, it's examined that up to how many EVs can charge it's battery under installed grid. This is an important decision stage in order to examine if proposed circuitry has any effects distortion of the supplied current or voltage and harmonics that formed by proposed circuitry, etc. on the installed grid of Çukurova University.

3. CONTROL TECHNIQUES

3.1. Controlled Rectifiers

3.1.1. Three-phase Full Converters

Three-phase converters are extensively used in industrial applications up to the 120-kW level, where a two-quadrant operation is required. Figure 3.1 shows a full-converter circuit with a highly inductive load.

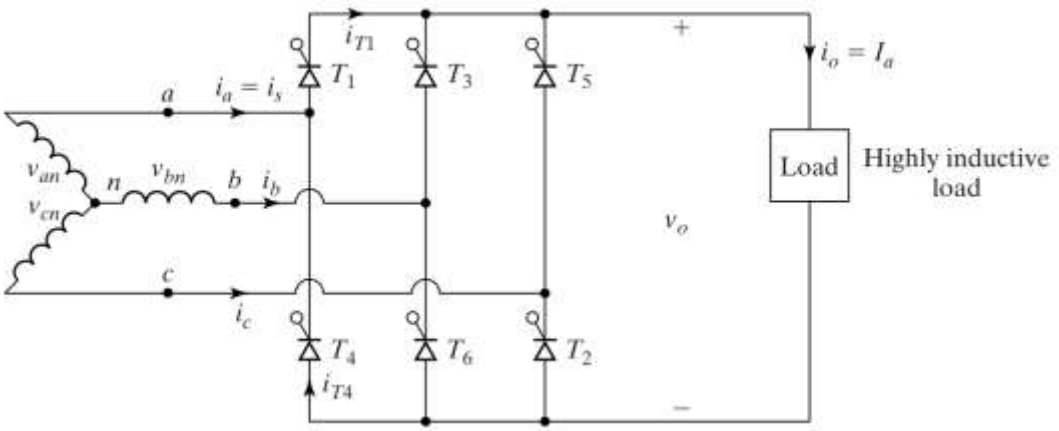

Figure 3.1. Three-phase full converter circuit (Rashid, 2014)

This circuit is known as a three-phase bridge. The thyristors are turned on at an interval of π/3. The frequency of output ripple voltage is $6f_s$ and the filtering requirement is less than that of half-wave converters. At $\omega t = \pi/6 + \alpha$, thyristor T_6 is already conducting and thyristor T_1 is turned on. During interval $(\pi/6 + \alpha) \leq \omega t \leq (\pi/2 + \alpha)$, thyristors T_1 and T_6 conduct and the line-to-line voltage υ_{ab} $(= \upsilon_{an} - \upsilon_{bn})$ appears across the load. At $\omega t = \pi/2 + \alpha$, thyristor T_2 is turned on and thyristor T_6 is reverse biased immediately. T_6 is turned off due to natural commutation. During interval $(\pi/2 + \alpha) \leq \omega t \leq (5\pi/6 + \alpha)$, thyristors T_1 and T_2 conduct and the line-to-line voltage υ_{ac} appears across the load. If the thyristors are numbered, as shown in Figure 3.2, the firing sequence is 12, 23, 34, 45, 56, and 61. Figure 3.2 also shows firing sequences

of thyristors and the waveforms for input voltage, output voltage, input current, and currents through thyristors (Rashid, 2014).

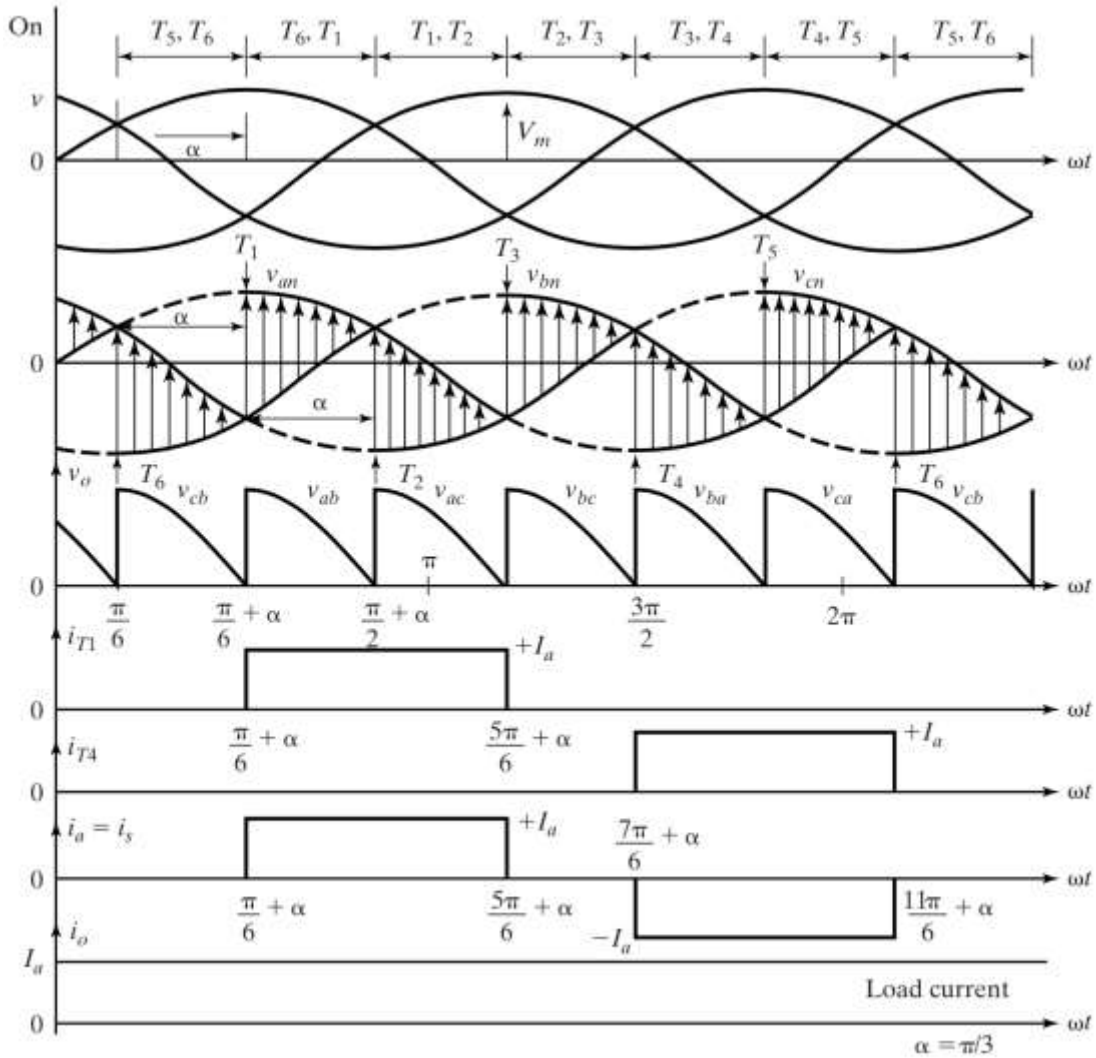

Figure 3.2. Three-phase full converter triggering sequences, phase voltages, output voltage (line-to-line voltages), current through thyristor T_1, current through thyristor T_2, input supply current and constant load current (from top to down) (Rashid, 2014)

If the line-to-neutral voltages are defined as

$$v_{an} = V_m \sin \omega t \tag{3.1}$$

$$v_{bn} = V_m \sin\left(\omega t - \frac{2\pi}{3}\right) \tag{3.2}$$

$$v_{cn} = V_m \sin(\omega t + \frac{2\pi}{3}) \tag{3.3}$$

the corresponding line-to-line voltages are

$$v_{ab} = v_{an} - v_{bn} = \sqrt{3}\, V_m \sin\left(\omega t + \frac{\pi}{6}\right) \tag{3.4}$$

$$v_{bc} = v_{bn} - v_{cn} = \sqrt{3}\, V_m \sin\left(\omega t - \frac{\pi}{2}\right) \tag{3.5}$$

$$v_{ca} = v_{cn} - v_{an} = \sqrt{3}\, V_m \sin\left(\omega t + \frac{\pi}{2}\right) \tag{3.6}$$

The average output voltage is found from

$$V_{\mathrm{dc}} = \frac{3}{\pi}\int_{\pi/6+\alpha}^{\pi/2+\alpha} v_{ab}\, d(\omega t) = \frac{3}{\pi}\int_{\pi/6+\alpha}^{\pi/2+\alpha} \sqrt{3} V_m \sin\left(\omega t + \frac{\pi}{6}\right) d(\omega t) \tag{3.7}$$

$$= \frac{3\sqrt{3}V_m}{\pi}\cos\alpha$$

The maximum average output voltage for delay angle, $\alpha = 0$, is

$$V_{dm} = \frac{3\sqrt{3}V_m}{\pi} \tag{3.8}$$

and the normalized average output is

$$V_n = \frac{V_{\mathrm{dc}}}{V_{dm}} = \cos\alpha \tag{3.9}$$

The rms value of the output voltage is found from

$$V_{\text{rms}} = \left[\frac{3}{\pi}\int_{\pi/6+\alpha}^{\pi/2+\alpha} \sqrt{3}V_m^2 \sin^2\left(\omega t + \frac{\pi}{6}\right) d(\omega t)\right]^{1/2}$$

$$= \sqrt{3}V_m \left(\frac{1}{2} + \frac{3\sqrt{3}}{4\pi}\cos 2\alpha\right)^{\frac{1}{2}} \quad (3.10)$$

Figure 3.2 shows the waveforms for $\alpha = \pi/3$. For $\alpha > \pi/3$, the instantaneous output voltage υ_o has a negative part. Because the current through thyristors cannot be negative, the load current is always positive. Thus, with a resistive load, the instantaneous load voltage cannot be negative, and the full converter behaves as a semi-converter (Rashid, 2014).

The gating sequence as follows:

1. Generate a pulse signal at the positive zero crossing of the phase voltage υ_{an}. Delay the pulse by the desired angle $\alpha + \pi/6$ and apply it to the gate and cathode terminals of T_1 through a gate-isolating circuit.
2. Generate five more pulses each delayed by $\pi/6$ from each other for gating T_2, T_3,…, T_6, respectively, through gate-isolating circuits (Buso and Mattavelli, 2006).

3.1.2. Three-phase Dual Converters

In many variable-speed drives, the four-quadrant operation is generally required and three-phase dual converters are extensively used in applications up to the 2000-kW level. Figure 3.3 shows three-phase dual converters where two three-phase converters are connected back to back. Due to the instantaneous voltage differences between the output voltages of converters, a circulating current flows through the converters. The circulating current is normally limited by circulating reactor L_r, as shown in Figure 3.4 (Luo, 2005).

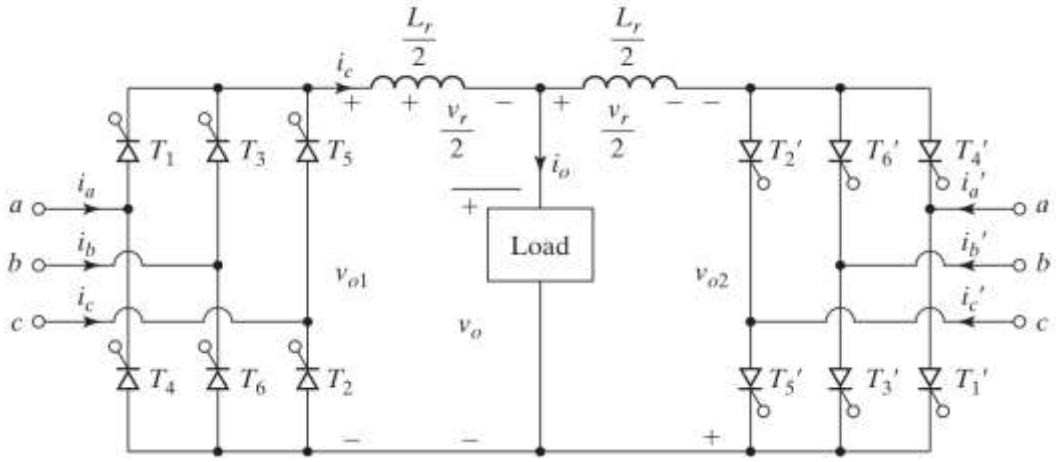

Figure 3.3. Three-phase dual converter circuit (Rashid, 2014)

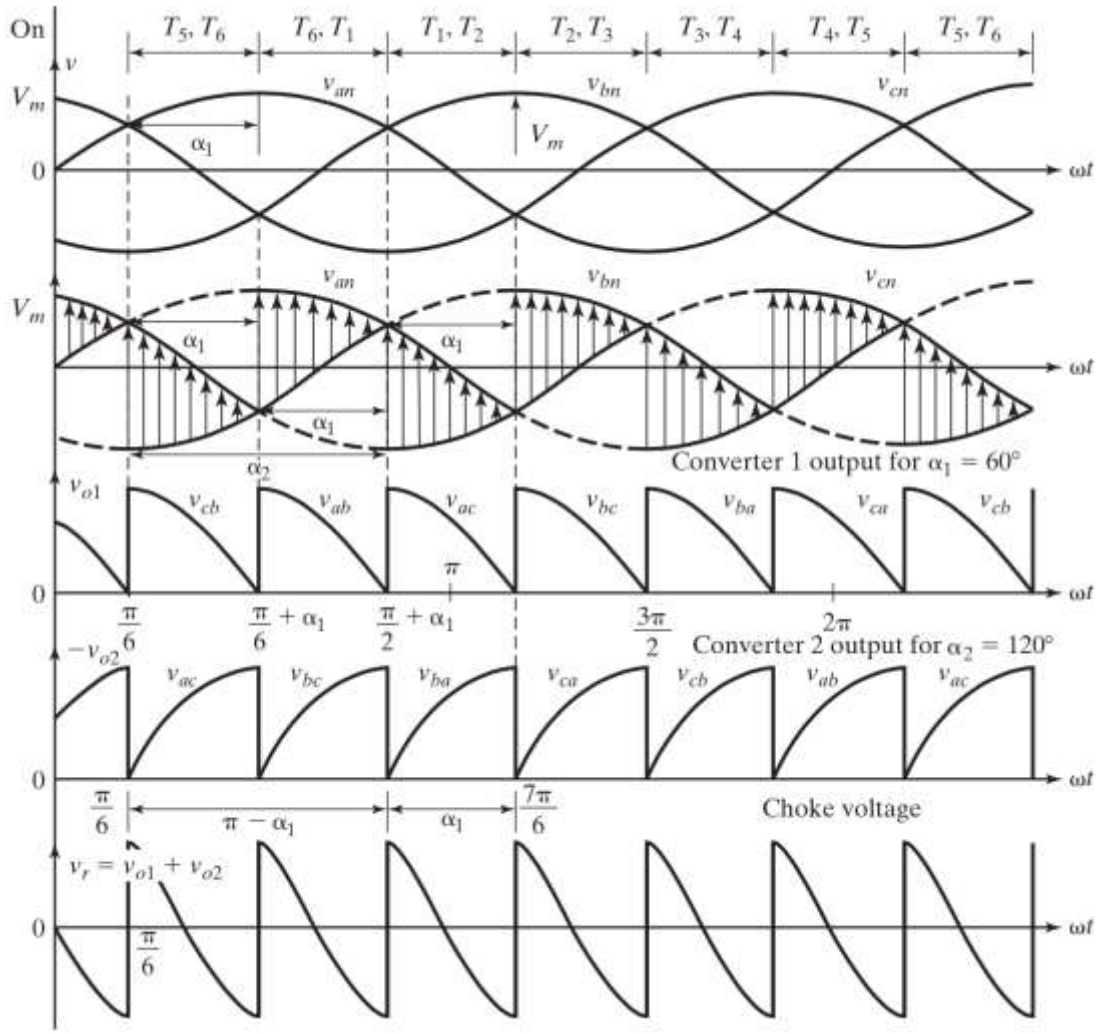

Figure 3.4. Three-phase dual converter triggering sequences, input supply voltages, output voltage for converter 1, output voltage for converter 2, and circulating voltage (from top to down) (Rashid, 2014)

The two converters are controlled in such a way that α_1 is the delay angle of converter 1, the delay angle of converter 2 is $\alpha_2 = \pi - \alpha_1$. Figure 3.4 shows the waveforms for input voltages, output voltages, and the voltage across inductor L_r. The operation of each converter is identical to that of a three-phase full converter. During the interval $(\pi/6 + \alpha_1) \leq \omega t \leq (\pi/2 + \alpha_1)$, the line-to-line voltage v_{ab} appears across the output of converter 1, and v_{bc} appears across converter 2 (Fewson, 1998).

If the line-to-neutral voltages are defined as

$$v_{an} = V_m \sin \omega t \tag{3.11}$$

$$v_{bn} = V_m \sin(\omega t - \frac{2\pi}{3}) \tag{3.12}$$

$$v_{cn} = V_m \sin(\omega t + \frac{2\pi}{3}) \tag{3.13}$$

the corresponding line-to-line voltages are

$$v_{ab} = v_{an} - v_{bn} = \sqrt{3}\, V_m \sin\left(\omega t + \frac{\pi}{6}\right) \tag{3.14}$$

$$v_{bc} = v_{bn} - v_{cn} = \sqrt{3}\, V_m \sin\left(\omega t - \frac{\pi}{2}\right) \tag{3.15}$$

$$v_{ca} = v_{cn} - v_{an} = \sqrt{3}\, V_m \sin\left(\omega t + \frac{5\pi}{6}\right) \tag{3.16}$$

If v_{o1} and v_{o2} are the output voltages of converters 1 and 2, respectively, the instantaneous voltage across the inductor during interval $(\pi/6 + \alpha_1) \leq \omega t \leq (\pi/2 + \alpha_1)$ is

$$v_r = v_{o1} + v_{o2} = v_{ab} + v_{bc} \tag{3.17}$$

$$= \sqrt{3} V_m \left[\sin\left(\omega t + \frac{\pi}{6}\right) - \sin\left(\omega t - \frac{\pi}{2}\right)\right] \tag{3.18}$$

$$= 3V_m \cos\left(\omega t + \frac{\pi}{6}\right) \tag{3.19}$$

The circulating current can be found from

$$i_r(t) = \frac{1}{\omega L_r}\int_{\pi/6+\alpha_1}^{\omega t} v_r d(\omega t) = \frac{1}{\omega L_r}\int_{\pi/6+\alpha_1}^{\omega t} 3V_m \cos\left(\omega t - \frac{\pi}{6}\right) d(\omega t) \tag{3.20}$$

$$= \frac{3}{\omega L_r}\left[\sin\left(\omega t - \frac{\pi}{6}\right) - \sin\alpha_1\right] \tag{3.21}$$

The circulating current depends on delay angle α_1 and on inductance L_r. This current becomes maximum when $\omega t = 2\pi/3$ and $\alpha_1 = 0$. Even without any external load, the converters would be continuously running due to the circulating current as a result of ripple voltage across the inductor. This allows smooth reversal of load current during the changeover from one quadrant operation to another and provides fast dynamic responses, especially for electrical motor drives (Rashid, 2014).

The gating sequence as follows:

1. Similar to the single-phase dual converter, gate positive converter with a delay angle of $\alpha_1 = \alpha$.
2. Gate the negative converter with a delay angle of $\alpha_2 = \pi - \alpha$ through gate-isolating circuits (Rashid, 2014).

3.1.3. Three-phase PWM Rectifier

There are two circuit topologies for three-phase rectifiers: (1) a current-source rectifier, where power reversal is done by dc voltage reversal; and (2) a voltage-source rectifier, where power reversal is by current reversal at the dc link. Figure 3.5 and Figure 3.6 show the basic circuits for these two topologies. Inductor L_D in Figure 3.5, maintains a constant current to the load while the input-side capacitors provide low impedance paths for the load current. Capacitor C_D in Figure 3.6, maintains a

constant voltage to the load while the input-side inductances ensure the continuity of the line currents and improve the input power factor (Kularanta, 1998).

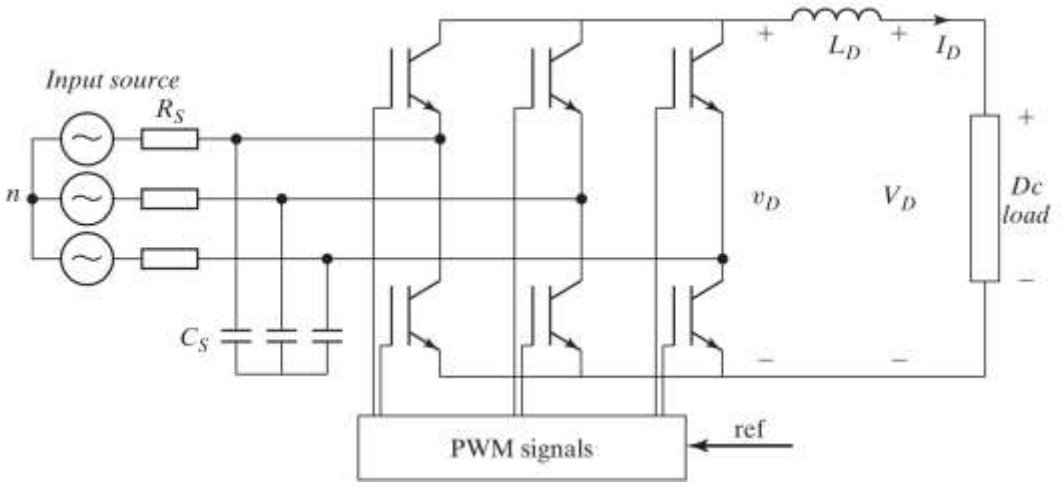

Figure 3.5. Current-source force commutated PWM rectifier (Rashid, 2014)

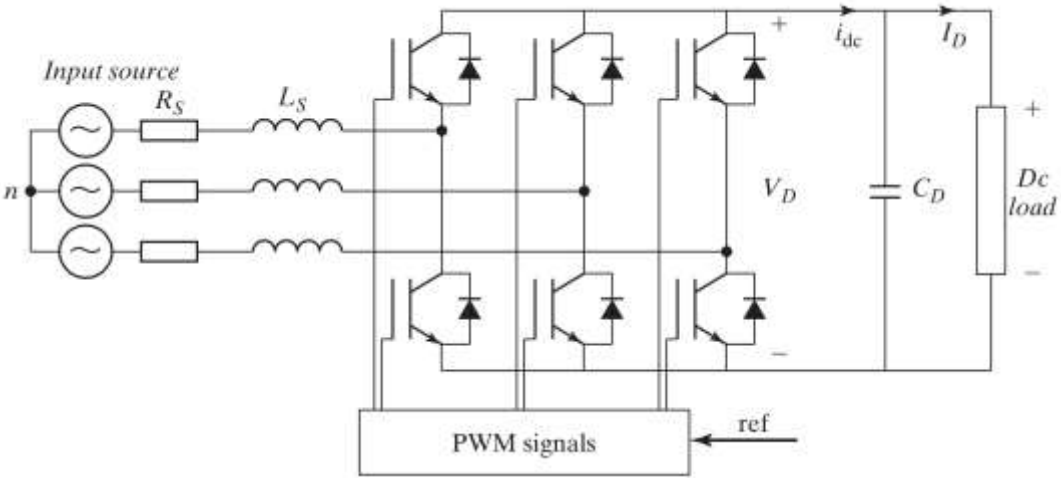

Figure 3.6. Voltage-source force commutated PWM rectifier (Rashid, 2014)

A three-phase voltage-source rectifier with a feedback control loop is shown in Figure 3.7. The dc-link voltage is maintained at a desired reference value by using a feedback control loop. It is measured and compared with a reference V_{ref}. The error signal switches on and off the six switching devices of the rectifier. The power flow from and to the ac source can be controlled according to the dc-link voltage requirements. The voltage V_D is measured at the dc-side capacitor C_D. Controlling

the dc-link voltage so that the current flow is reversed at the dc-link can control the power reversal (Sueker, 2005).

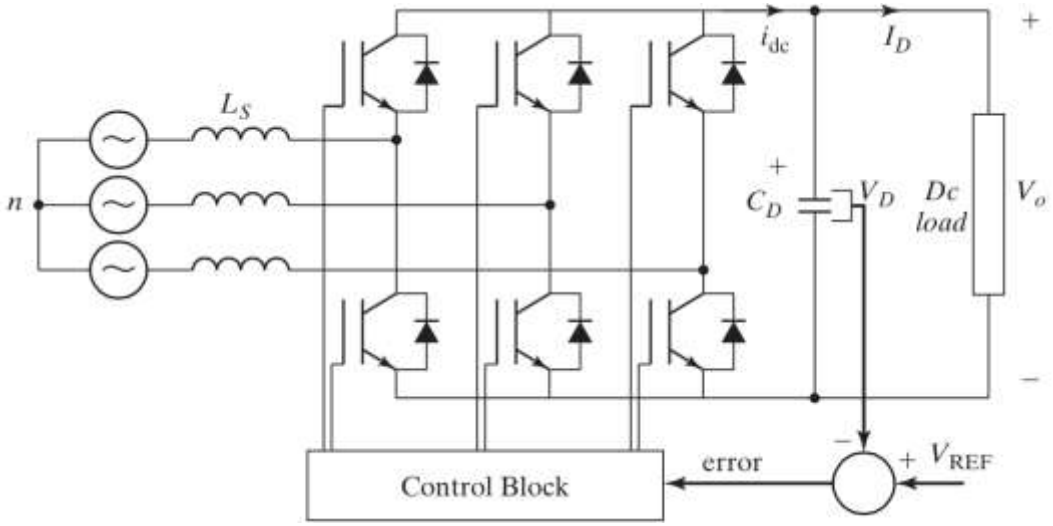

Figure 3.7. Forced-commutated voltage-source rectifier circuit (Rashid, 2014)

In the rectifier mode of operation, the current I_D is positive and the capacitor C_D is discharged through the dc load, and the error signal demands the control circuit for more power from the ac power supply. The control circuit takes the power from the supply by generating the appropriate PWM signals for the switching devices. More current flows from the ac to the dc side, and the capacitor voltage is recovered. In the inverter mode of operation I_D becomes negative and the capacitor C_D is overcharged. The error signal demands the control to discharge the capacitor and return power to the ac mains (Williams, 1992).

The PWM can control both the active power and reactive power. Thus, this type of rectifier can be used for PF correction. The ac current waveforms can also be maintained almost sinusoidal, reducing harmonic contamination to the mains supply. The PWM turns on and off the switches in a pre-established form, usually a sinusoidal waveform of voltage or current. An example of the modulation of one phase is shown in Figure 3.8 with amplitude of V_{MOD} for the modulating signal (Rashid, 2014).

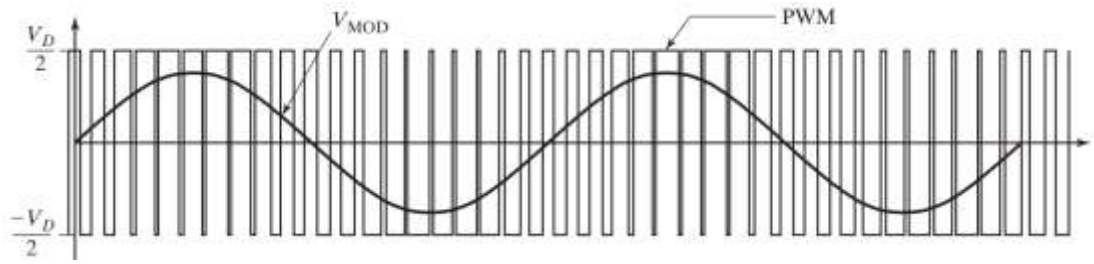

Figure 3.8. Forced-commutated voltage-source rectifier PWM pattern and its fundamental modulating V_{MOD} (Rashid, 2014)

Depending on the control strategy, a force-commutated rectifier can be operated as either an inverter or a rectifier. Therefore, it is often referred to as a converter. Two such converters are often cascaded to control power flow from the ac supply to the load and vice versa, as shown in Figure 3.9. The first converter converts ac to a variable dc-link voltage and the second converter converts dc to a variable ac at fixed or variable frequency. Advanced control techniques (e.g., space vector modulation and SPWM) can maintain a near sinusoidal input current from the ac source at unity PF and supply a near sinusoidal output voltage or current to the load. Advanced control techniques can be used to generate three-phase output from a single-phase supply.

Main advantages include:

- The current or voltage can be modulated, generating less harmonic contamination.
- The PF can be controlled, and it even can be made leading.
- The circuit can be built as voltage-source or current-source rectifiers.
- The PF can be reversed by reversing the current at the dc-link (Rashid, 2014).

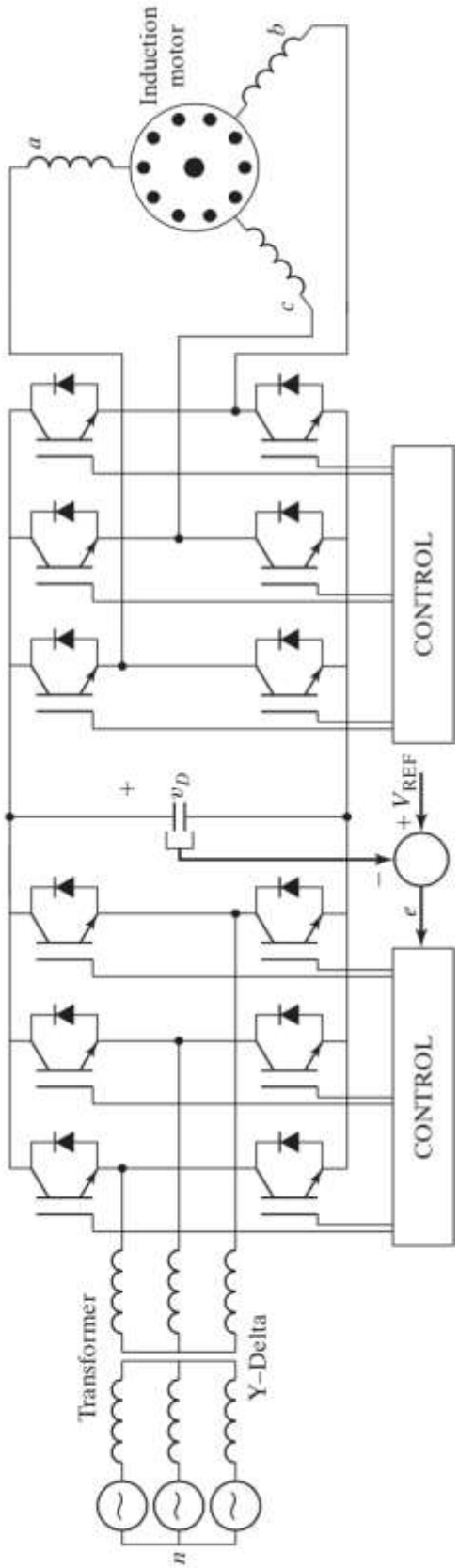

Figure 3.9. Two forced-commutated cascaded converters (Rashid, 2014)

3.2. DQ Theory

Direct–quadrature–zero (or dq0 or dqo) transformation or zero–direct–quadrature (or 0dq or odq) transformation is a mathematical transformation that rotates the reference frame of three-phase systems in an effort to simplify the analysis of three-phase circuits. A balanced three-phase circuit, dqo conversion application reduces three AC components to the two DC components. Simplified calculations can be done on the DC components before applying the inverse transform to actual three-phase AC results.

The synchronous reference frame method is based on the transformation of vectors into synchronously rotating direct (d), and quadrature axis (q) reference frames. Initially three phase supply current vectors are mapped into synchronously rotating reference frame in (3.22). The phase angle θ defines the fundamental frequency phase information of the utility voltage and it is obtained from a phase locked loop circuit which is investigated.

$$\begin{bmatrix} i_d \\ i_q \\ i_0 \end{bmatrix} = \sqrt{\frac{2}{3}} \begin{bmatrix} \cos\phi & \cos(\phi - \frac{2\pi}{3}) & \cos(\phi + \frac{2\pi}{3}) \\ -\sin\phi & -\sin(\phi - \frac{2\pi}{3}) & -\sin(\phi + \frac{2\pi}{3}) \\ \frac{\sqrt{2}}{2} & \frac{\sqrt{2}}{2} & \frac{\sqrt{2}}{2} \end{bmatrix} \tag{3.22}$$

$$\begin{bmatrix} i_a \\ i_b \\ i_c \end{bmatrix} = \sqrt{\frac{2}{3}} \begin{bmatrix} \cos\phi & -\sin\phi & \frac{\sqrt{2}}{2} \\ \cos(\phi - \frac{2\pi}{3}) & -\sin(\phi - \frac{2\pi}{3}) & \frac{\sqrt{2}}{2} \\ \cos(\phi + \frac{2\pi}{3}) & -\sin(\phi + \frac{2\pi}{3}) & \frac{\sqrt{2}}{2} \end{bmatrix} \tag{3.23}$$

Once the current vectors are transformed into synchronously rotating d-q reference frame, the fundamental component of the mains current turns out to be a DC signal, and the harmonic components which are still AC signals are rotating with a corresponding angular frequency as shown in Figure 3.10.

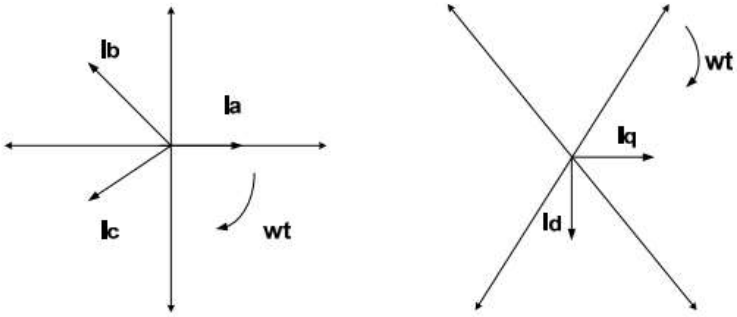

Figure 3.10. (a) Three Phase Current Vectors (b) DQ Transformation (Anderson and Fouad, 2002)

3.3. PID Controller

3.3.1. Proportional Control

A proportional controller is defined to be one in which the output is simply proportional to the input, where the constant of proportionality is the gain of the controller. Consider initially the first-order system with a disturbance input, shown in Figure 3.11.

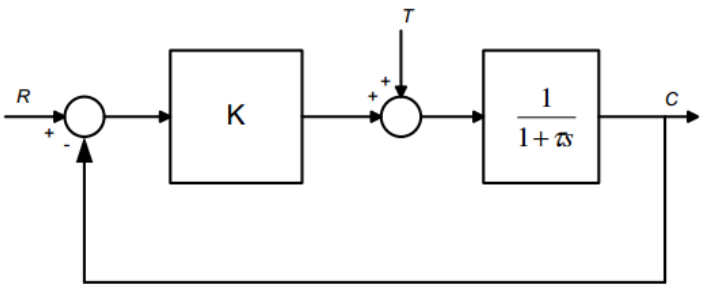

Figure 3.11. First order system with disturbance (Driels, 1996)

The transfer function relating output *C* to the two inputs *R* and *T* are

$$\frac{C}{R} = \frac{K/(1+K)}{1+\tau s/(1+K)} \tag{3.24}$$

$$\frac{C}{T} = \frac{1/(1+K)}{1+\tau s/(1+K)} \tag{3.25}$$

If the input R is a unit step, the steady-state output becomes

$$c_{ss}(t) = \frac{K}{1+K} \tag{3.26}$$

If the disturbance T is a unit step, the corresponding steady-state output becomes

$$c_{ss}(t) = \frac{1}{1+K} \tag{3.27}$$

If K is made large, the output for unit R approaches unity, while the output for T approaches zero, which is a good result, but note that the error cannot be made equal to zero, since there will be practical limits on the magnitude of K. Consider a second order system, also subjected to external disturbance, as shown in Figure 3.12.

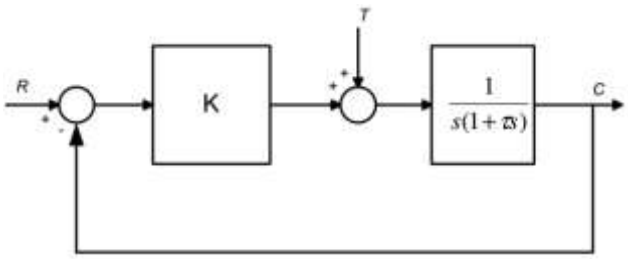

Figure 3.12. Second order system with disturbance (Driels, 1996)

The transfer functions from two inputs R and T to the output C as

$$\frac{C}{R} = \frac{K}{\tau s^2 + s + K} \tag{3.28}$$

$$\frac{C}{T} = \frac{1}{\tau s^2 + s + K} \tag{3.29}$$

The steady-state output for a unit step input R is

$$c_{ss}(t) = 1 \tag{3.30}$$

and for a unit step disturbance T it is

$$c_{ss}(t) = \frac{1}{K} \tag{3.31}$$

The steady-state error for the regular input is zero, as expected, but the disturbance does produce a finite error. Although this may be made small by letting K is large. Simple proportional control is of limited success is trying to obtain good performance in terms of steady-state error, disturbance rejection and transient response (Driels, 1996).

3.3.2. Proportional - Integral Control

A proportional – integral controller, where the output is proportional to the input plus the integral value of the input. This type of control is called two-mode control. The transfer function is seen to be

$$\theta_0 = \left[K_p + \frac{K_i}{s} \right] \theta_i \tag{3.32}$$

Consider this controller replaces proportional controller in the first order system. The new system looks like that shown in Figure 2.10. The new transfer function relating the output to the two inputs become,

$$\frac{C}{R} = \frac{K_p s + K_i}{\tau s^2 + s(1 + K_p) + K_i} \tag{3.33}$$

$$\frac{C}{T} = \frac{s}{\tau s^2 + s(1 + K_p) + K_i} \tag{3.34}$$

When the input R is a unit step, the steady-state output C becomes

$$c_{ss}(t) = 1 \tag{3.35}$$

and the steady-state output for unit T is

$$c_{ss}(t) = 0 \tag{3.36}$$

Proportional plus integral control has reduced the steady-state error to zero and completely rejected the external disturbance.

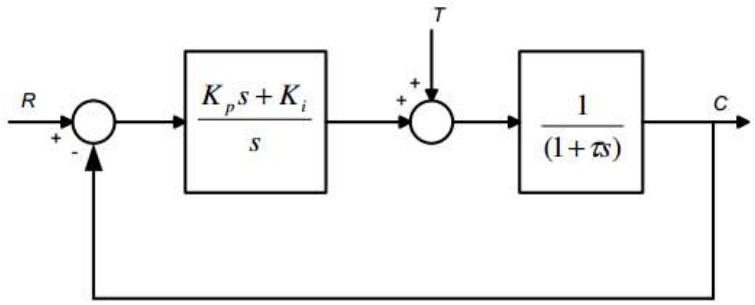

Figure 3.13. PI control of first-order system (Driels, 1996)

If the transfer function is second-order system as shown in Figure 2.11. The transfer function become

$$\frac{C}{R} = \frac{K_p s + K_i}{\tau s^3 + s^2 + sK_p + K_i} \tag{3.37}$$

$$\frac{C}{T} = \frac{s}{\tau s^3 + s^2 + sK_p + K_i} \tag{3.38}$$

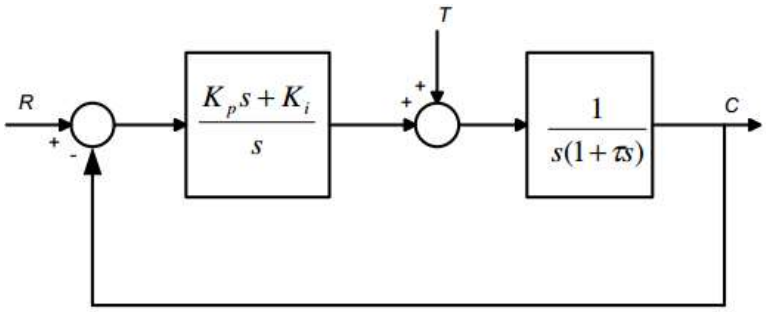

Figure 3.14. PI control of second order system (Driels, 1996)

Letting R be a unit step produces

$$c_{ss}(t) = 1 \tag{3.39}$$

and for the unit disturbance

$$c_{ss}(t) = 0 \tag{3.40}$$

Using the open-loop transfer function

$$GH(s) = \frac{K_p s + K_i}{s^2(1+\tau s)} \tag{3.41}$$

From the transfer function, its seen that the system has double pole at the origin, another pole at, and a zero at $s = 1/\tau$, and a zero at $s = -K_i / K_p$. In order for the system to be stable, the zero must be closer to the imaginary axis than the system pole.

$$\left|\frac{1}{\tau}\right| > \left|\frac{K_i}{K_p}\right| \tag{3.42}$$

This places some restrictions on the selection of the proportional and integral gains (Driels, 1996).

3.3.3. Proportional – Integral - Derivative Control

The transfer function of a PID (Proportional-Integral-Derivative) is may be written as

$$\frac{\theta_o}{\theta_i} = K_p + \frac{K_i}{s} + K_d s \tag{3.43}$$

PID controllers are very effective in adjusting the performance of control systems, and they are available as commercial components intended to be added to the forward path of a control system in order to improve its performance. Selection of values for K_p, K_i and K_d is known as tuning the controller, and it may be accomplished in many ways. The transfer function can be rewritten as (Driels, 1996).

$$\frac{\theta_o}{\theta_i} = K_p (1 + \frac{1}{T_i s} + T_d s) \tag{3.44}$$

4. MODELING OF FAST DC CHARGER CIRCUIT AND GRID INTEGRATION CIRCUIT

4.1. Fast DC Charger Circuit and Grid Integration Circuit Model

In this chapter, design and parameters of the Çukurova University's grid, charging circuits, charging methods and battery parameters will be described. Design of the grid simulation is made on the Çukurova University's one line diagram and includes actual values. Parameter values that used in simulation are also actual values too. Most basic aim of this simulation is to establish an electric vehicle infrastructure. Afterwards, by replacing the internal combustion engine vehicles that plying to Çukurova University with electric vehicles, it's aimed to reduce green-gas emissions (zero-emission by EVs, and less green-gas emissions by ICE), reduce the negative environmental effects and increased energy efficiency.

4.1.1. Grid Integration Circuits and Grid Parameters

Since, grid is simulated on a HV/LV single line diagram of the Çukurova University together with the loads all transformers used in this simulation are simulated with their actual values (Figure 4.1). All transformers are 33,5 kV/400 V power transformers. All RL blocks seen before the every transformer block represents the voltage drop of the relevant transformer. These RL blocks' values are calculated according to the type of cables used and the distance between transformers and the main supply (Figure 4.2). Proper places for charging stations are envisaged to be on the road in front of the Food engineering Department of the Faculty of Agriculture which is closer to Faculty of Agriculture Transformer 1 and will be supplied by Faculty of Agriculture Transformer 1.

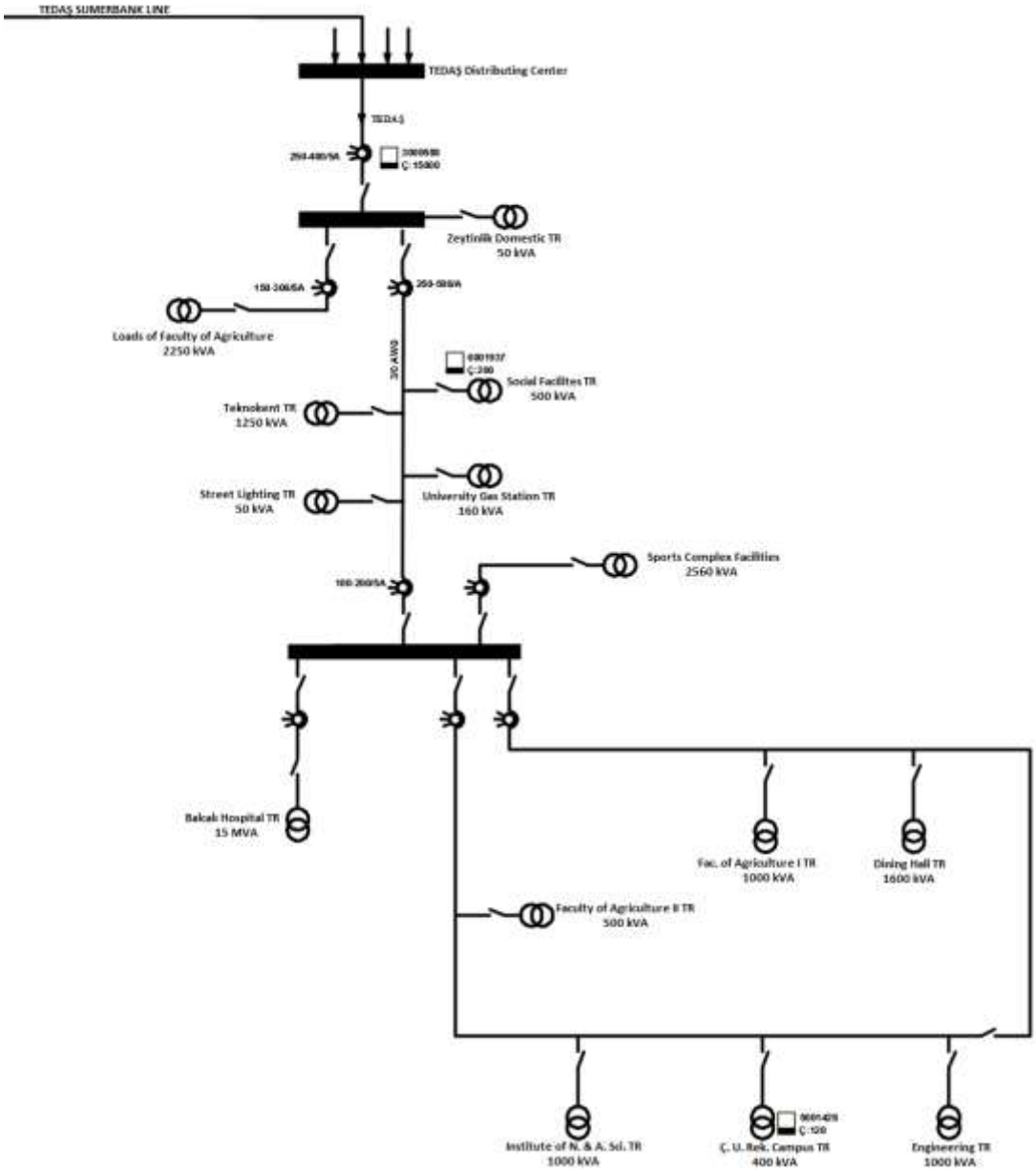

Figure 4.1. Çukurova University HV/LV One Line Diagram

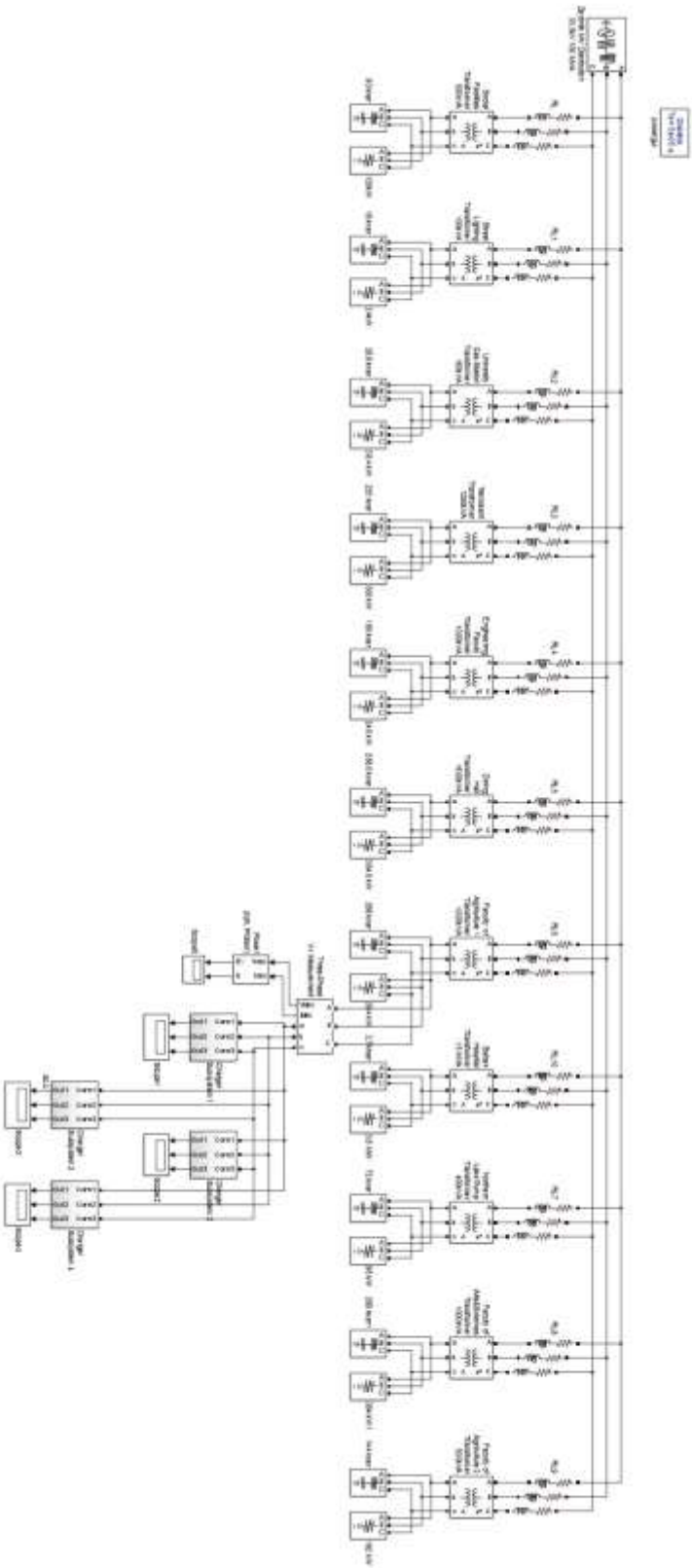

Figure 4.2. Grid integration and charger circuit diagram MatLab / Simulink

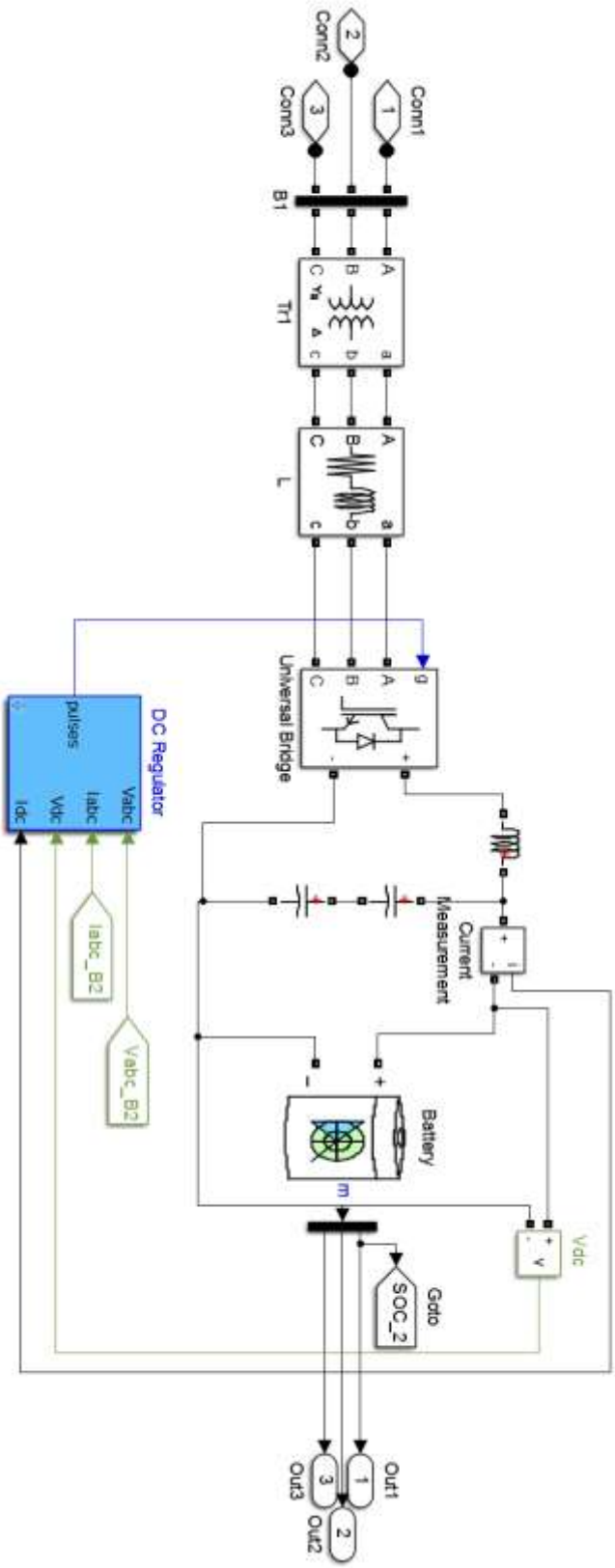

Figure 4.3. Charger circuit MatLab / Simulink

4.1.2. Charger Circuit

400V 3 phase grid signals are sent through transformer block to rectifier block. Rectifier block perform the AC-DC conversion by the triggers received from the controller and afterwards transmits DC voltage to the battery via the DC link (Figure 4.3).

4.1.2.1. Constant Current / Constant Voltage Controller

In constant current/constant voltage controller method, battery charges up to %95 SOC in constant current mode, then switches to constant voltage method, where it completes its charging period (%100 SOC). During constant current mode, DC Current Regulator Block produces the error signal by comparing reference current with measured current. This error signal sends to PI Block in order to produce Vd_ref signal which is the d component of voltage. During constant voltage mode, DC Voltage Regulator Block produces the error signal by comparing reference voltage with measured voltage. This error signal sends to PI Block in order to produce Id_ref signal which is the d component of current. These two data are compared in comparator block by the data signal of state of charge of the battery and data signal from battery block makes the selection between constant current and constant voltage charging modes (Figure 4.4).

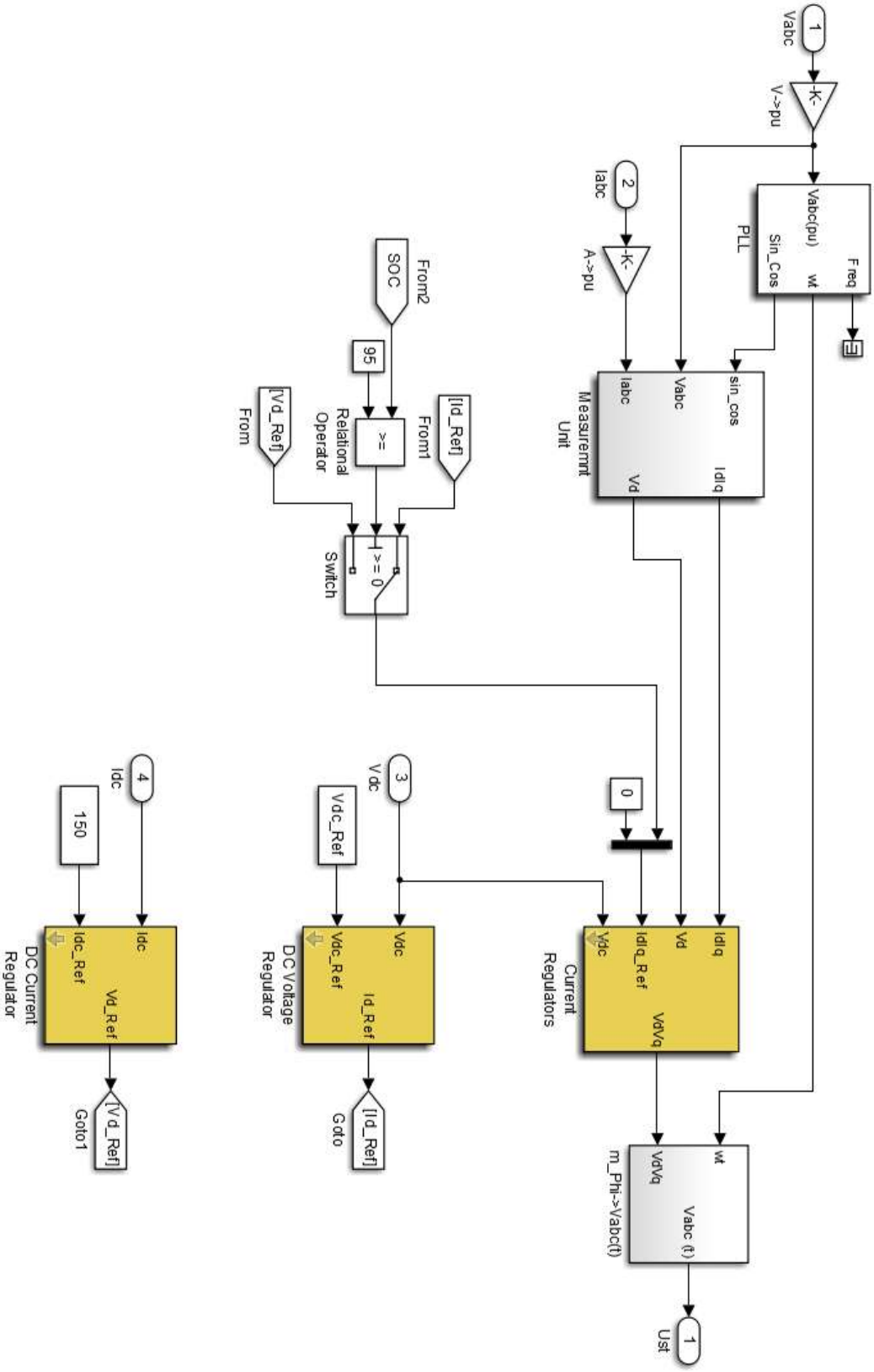

Figure 4.4. Constant Current-Constant Voltage Controller MatLab / Simulink

4.1.3. Battery Parameters

The battery used in our simulation has 440 V nominal voltage, 240 Ah rating. In real, this battery pack consists of four parallel lines each including 138 batteries with 3,2 V nominal voltage in series. Thus design gives us the chance of charging this battery up to 240 A. With these given values an empty EV can cruise up to 120 km. However, at full passenger capacity with full load (air-conditioner on, etc.), EV can cruise around 60 km.

5. CASE STUDIES

In this chapter, several case studies on different charging scenarios are introduced. These scenarios consist of inclusion of electric vehicle (EV) to the existing bus lines plying to the Çukurova University.

Among 18 bus lines, 10 lines are chosen and any chosen line is considered to have only one EV included. In any bus line, it is assumed to have X number of internal combustion engine (ICE) buses. Thus, any chosen bus line has X+1 number of vehicles. In the scenario, while EV is plying its route, one ICE vehicle removed from the fleet and added again while EV is charging its battery.

When EV is on track, it starts with 100% state of charge (SOC). After completing its route, EV is removed from the fleet in order to charge its battery. While EV is charging, X numbers of buses keep plying their regular route. When EV has recharged its battery and reached to 100% SOC, one ICE vehicle discarded from the fleet and EV is included again.

In this thesis, 5 cases are investigated in order to examine the system in detail and to see effects of the proposed infrastructure on the system, gradually. These cases are:

- Case 1: 2 chosen bus lines,
- Case 2: 4 chosen bus lines,
- Case 3: 6 chosen bus lines,
- Case 4: 8 chosen bus lines,
- Case 5: 10 chosen bus lines.

It's foreseen that charging stations will be placed on the road in front of Department of Food Engineering, Faculty of Agriculture. Four charging stations will be placed on the road in proper places and EVs after completion of their courses will come and recharge their batteries (Figure 5.1).

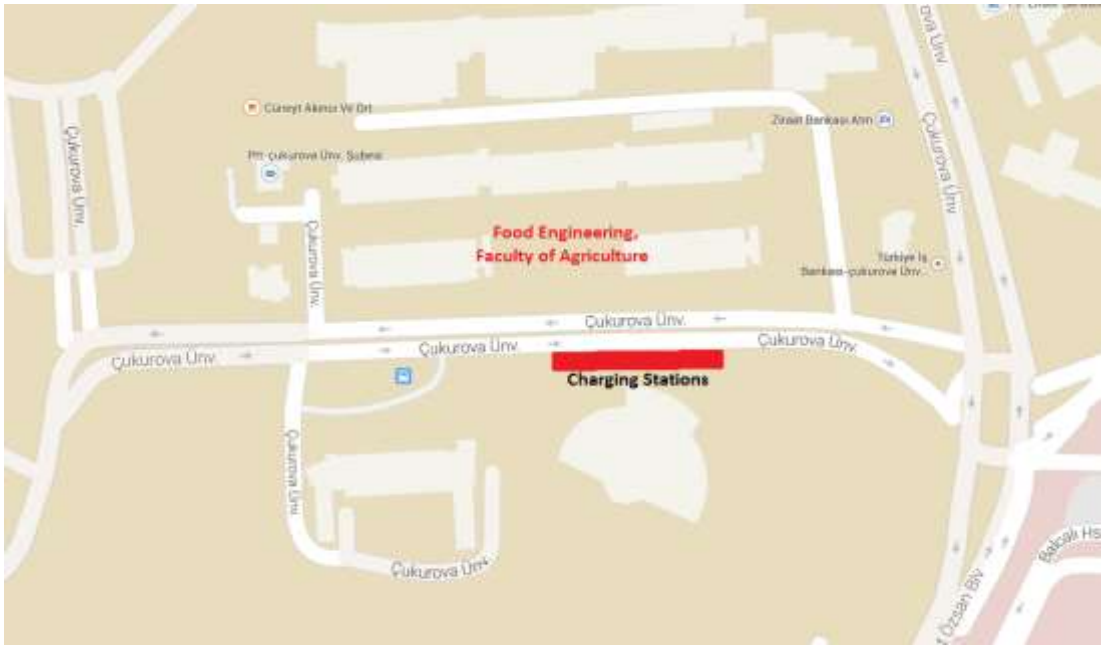

Figure 5.1. Foreseen charging stations' location in Çukurova University

Selection of bus lines that are plying to the Çukurova University are performed by taking into account the criteria such as emphasis, intensity, and length of course (e.g. route of line 192 is about 125 km long which overcomes the battery's maximum capacity). Plying hours, charging hours and daily total plying times are given in the Table 5.1.

Table 5.1. Bus Lines, Routes, Plying Hours, and Charging Times

Bus Line No	**113**	**116**	**121**	**122**	**133**
Route -SOC	30km - %50 SOC	45km - %75 SOC	40km - %66 SOC	50km - %80 SOC	45km - %75 SOC
1. tour	06:15-08:15	06:23-08:30	07:30-09:30	06:00-08:00	07:10-09:10
Charge	08:15-09:05	08:30-09:45	09:30-10:40	08:00-09:20	09:10-10:25
2. tour	09:15-11:15	10:13-12:15	11:30-13:30	10:00-12:00	10:28-12:30
Charge	11:15-12:05	12:15-13:30	13:30-14:40	12:00-13:20	12:30-13:45
3. tour	12:15-14:15	14:03-16:00	15:30-17:30	14:00-16:00	13:46-15:45
Charge	14:30-15:20	16:00-17:15	17:30-18:40	16:00-17:20	15:45-17:00
4. tour	15:25-17-25	17:53-20:00	-	18:00-20:00	17:04-19:04
Charge	17:25-18:15	-	-	-	-
5. tour	18:15-20:15	-	-	-	-
Charge	-	-	-	-	-
Bus Line No	**135**	**154**	**155**	**156**	**160**
Route -SOC	25km - %45 SOC	22km - %36 SOC	35km - %60 SOC	40km - %66 SOC	45km - %75 SOC
1. tour	10:00-12:00	06:00-08:00	08:00-10:00	08:05-10:05	06:54-09:00
Charge	12:00-12:45	08:00-08:40	10:15-11:15	10:05-11:15	9:00-10:15
2. tour	13:00-15:00	09:00-11:00	11:30-13:30	12:05-14:00	10:30-12:30
Charge	15:00-15:45	11:00-11:40	13:30-14:30	14:00-15:10	12:45-14:00
3. tour	16:00-18:00	12:00-14:00	15:00-17:00	16:05-18:00	14:06-16:10
Charge	18:00-18:45	14:00-14:40	17:00-18:00	18:00-19:05	16:10-17:25
4. tour	19:00-21:00	15:00-17:00	18:30-20:30	19:05-21:00	17:42-19:45
Charge	-	17:15-17:55	-	-	-
5. tour	-	18:00-20:00	-	-	-
Charge	-	-	-	-	-

Taking into account the information given in the Table 4.1, while the busiest scenario (Case 5) is being processed, there are two situations that are foreseen as a possible problem to arise. These situations are:

Situation 1: Whether there are sufficient numbers of charging stations while EVs are charging.

Situation 2: Prediction of the optimum number of charging stations.

These situations are examined under the guidance of the given information below:

1. Duration between battery charge process and next plying time,
2. The average time to complete each vehicle's route,
3. Hourly/daily (rush hours/eves of holidays) density condition of traffic,
4. Even an EV is planned to be charged right after completion of its course, the charging process might be delayed when the following situations occur simultaneously:
    4.1. Presence of a relatively long waiting time between the end of charging process and next plying hour.
    4.2. Number of concurrently incoming EVs exceeds the number of available charging stations.
5. EVs with shorter route (e.g. SOC consumption < 50%) may leave the charging stations before reaching 100% SOC when charging stations are busy,

for such reasons, it is possible to ignore the minor overlaps in charging times given in the Table 5.2 and four charging stations are predicted to be sufficient for the maximum number of stations.

Table 5.2. Charging list of the bus lines

HOURS	STATION 1	STATION 2	STATION 3	STATION 4
08:00	154	122		
08:15	154	122	113	
08:30	154	122	113	116
08:45		122	113	116
09:00	160	122	113/133	116
09:15	160	122	133	116
09:30	160	121	133	116
09:45	160	121	133	
10:00	160	121	133	156
10:15	155	121	133	156
10:30	155	121		156
10:45	155			156
11:00	155	154		156
11:15		154	113	
11:30		154	113	
11:45			113	
12:00	135	122	113	
12:15	135	122		116
12:30	135	122	133	116
12:45	160	122	133	116
13:00	160	122	133	116
13:15	160	122	133	116
13:30	160	121	133	155
13:45	160	121		155
14:00	154	121	156	155
14:15	154	121	156	155
14:30	154	121	156	113
14:45			156	113
15:00	135		156	113
15:15	135			113
15:30	135			
15:45			133	
16:00	160	122	133	116
16:15	160	122	133	116
16:30	160	122	133	116
16:45	160	122	133	116
17:00	160	122		116/155
17:15	154	122	113	155
17:30	154	121	113	155
17:45	154	121	113	155
18:00	135	121	113	156
18:15	135	121		156
18:30	135	121		156
18:45				156
19:00				156

5.1. Case 1: Two Electric Vehicles Charge

First bus line among the chosen bus lines is line 154. In line 154, every vehicle completes its tour in 60+60 minutes (from departure to arrival). First EV in the morning starts its route at 06:00, plying ends at 08:00 and connects to charging station. A battery's charging time takes up to 100 minutes (from 0% to 100%). In line 154, after completing a full route, 36% SOC will be used and in order to replenish the missing SOC approximately 35-40 minutes of charging will be required. This calculation can be basically described as; a full route's distance (in km) divided by maximum distance cruised (in km) with a fully charged battery. Based on this information, it will take up to sixty minutes for an EV to join the fleet again after recharging its battery to the state of 100% SOC. Next plying will take place sixty minutes ahead of beginning of the charging process. So, EV will be active in fleet again at 09:00. When EV is in fleet, an ICE vehicle will be discarded again. If this loop continues in that way, EV in line 154 will be active in fleet at 12:00, 15:00 and 18:00. Since last plying takes place at 19:00, EV in line 154 makes 5 plyings during the day.

Second bus line among the chosen bus lines is line 113. In line 113, every vehicle completes its tour in 60+60 minutes (from departure to arrival). First EV in the morning starts its route at 06:15, plying ends at 08:15 and then connects to charging station. In line 113, after completing a full route, 50% SOC will be used and in order to replenish the missing SOC approximately 50 minutes of charging will be required. EV in line 113 will be active in fleet at 09:15, 12:15, 15:25 and 18:15. Since last plying takes place at 19:00, EV in line 113 makes 5 plyings during the day.

5.2. Case 2: Four Electric Vehicles Charge

Additional 2 lines to Case 1 will be added to scenario. First added bus line is line 116. In line 116, every vehicle completes its tour in 60+60 minutes (from departure to arrival). First EV in the morning starts its route at 06:23, plying ends at around 08:30 and connects to charging station. In line 116, after completing a full

route, 75% SOC will be used and in order to replenish the missing SOC approximately 75 minutes of charging will be required. EV in line 116 will be active in fleet at 10:13, 14:03 and 17:53. Since last plying takes place at 19:25, EV in line 116 will be made 4 plyings during the day.

Second added bus line is line 121. In line 121, every vehicle completes its tour in 60+60 minutes (from departure to arrival). First EV in the morning starts its route at 07:30, plying ends at around 09:30 and connects to charging station. In line 121, after completing a full route, 66% SOC will be used and in order to replenish the missing SOC approximately 65-70 minutes of charging will be required. EV in line 121 will be active in fleet at 11:30 and 13:30. Since last plying takes place at 18:30, EV in line 121 will be made 3 plyings during the day.

5.3. Case 3: Six Electric Vehicles Charge

Additional 2 lines to Case 2 will be added to scenario. First added bus line is line 122. First EV in the morning starts its route at 06:00, plying ends at around 08:00 and connects to charging station. In line 122, after completing a full route, 80% SOC will be used and in order to replenish the missing SOC approximately 80 minutes of charging will be required. EV in line 122 will be active in fleet at 10:00, 14:00 and 18:00. Since last plying takes place at 18:00, EV in line 122 will be made 4 plyings during the day.

Second added bus line is line 133. First EV in the morning starts its route at 07:10, plying ends at around 09:10 and connects to charging station. In line 133, after completing a full route, 75% SOC will be used and in order to replenish the missing SOC approximately 75 minutes of charging will be required. EV in line 133 will be active in fleet at 10:28, 13:46 and 17:04. Since last plying takes place at 17:04, EV in line 133 will be made 4 plyings during the day.

5.4. Case 4: Eight Electric Vehicles Charge

Additional 2 lines to Case 3 will be added to scenario. First added bus line is line 135. First EV in the morning starts its route at 10:00, plying ends at around 12:00 and connects to charging station. In line 135, after completing a full route, 45% SOC will be used and in order to replenish the missing SOC approximately 45 minutes of charging will be required. EV in line 135 will be active in fleet at 13:00, 16:00 and 19:00. Since last plying takes place at 19:00, EV in line 135 will be made 4 plyings during the day.

Second added bus line is line 155. First EV in the morning starts its route at 08:00, plying ends at around 10:00 and connects to charging station. In line 155, after completing a full route, 60% SOC will be used and in order to replenish the missing SOC approximately 60 minutes of charging will be required. EV in line 155 will be active in fleet at 11:30, 15:00 and 18:30. Since last plying takes place at 19:30, EV in line 155 will be made 4 plyings during the day.

5.5. Case 5: Ten Electric Vehicles Charge

Additional 2 lines to Case 4 will be added to scenario. First added bus line is line 156. First EV in the morning starts its route at 08:05, plying ends at around 10:00 and connects to charging station. In line 156, after completing a full route, 66% SOC will be used and in order to replenish the missing SOC approximately 65-70 minutes of charging will be required. EV in line 156 will be active in fleet at 12:05, 16:05 and 19:05. Since last plying takes place at 19:05, EV in line 156 will be made 4 plyings during the day.

Second and the last added bus line to the scenario is line 160. First EV in the morning starts its route at 06:54, plying ends at around 09:00 and connects to charging station. In line 160, after completing a full route, 75% SOC will be used and in order to replenish the missing SOC approximately 75 minutes of charging will be required. EV in line 160 will be active in fleet at 10:30, 14:06 and 17:42. Since

last plying takes place at 19:30, EV in line 160 will be made 4 plyings during the day.

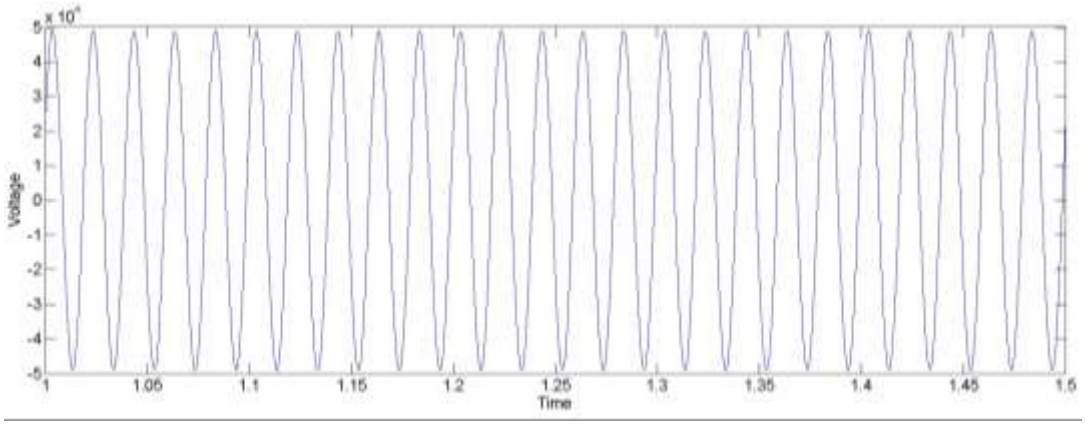

Figure 5.2. Main supply voltage

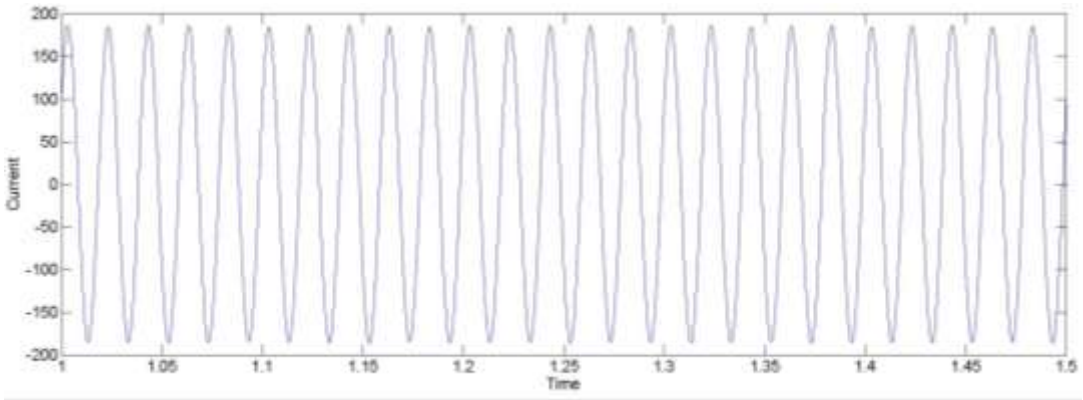

Figure 5.3. Main supply current

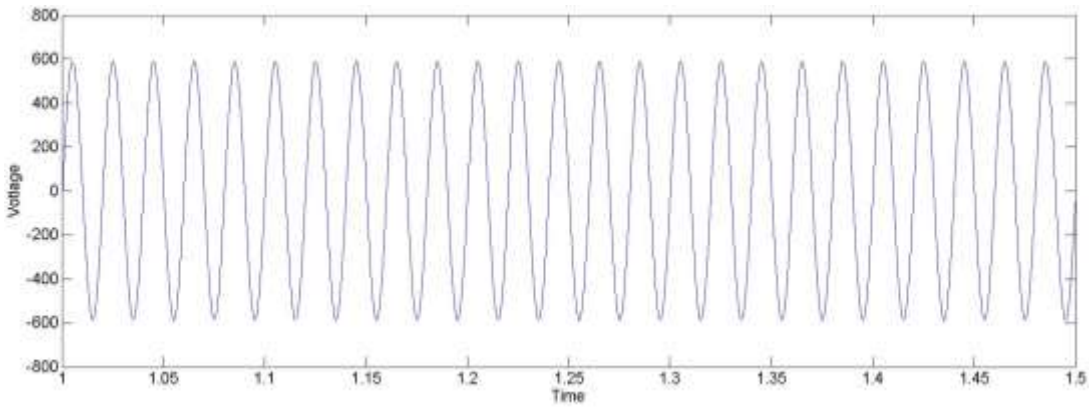

Figure 5.4. Balcalı hospital transformer voltage

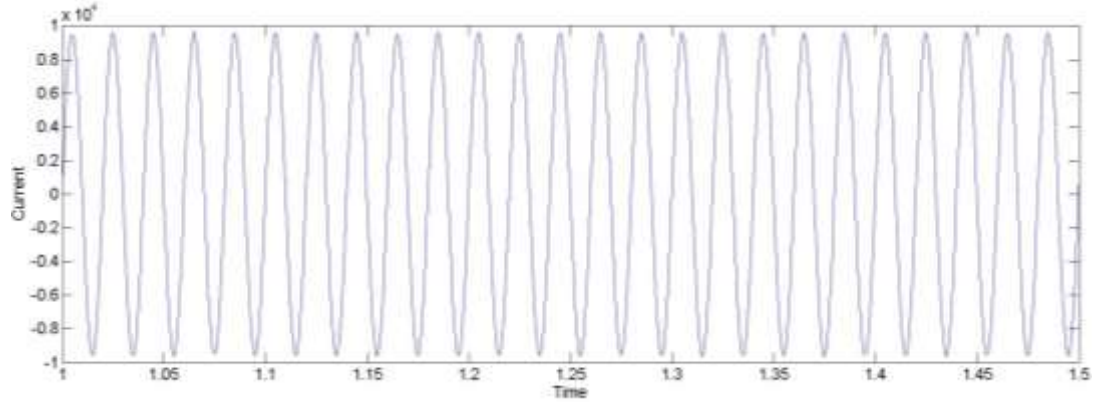

Figure 5.5. Balcalı hospital transformer current

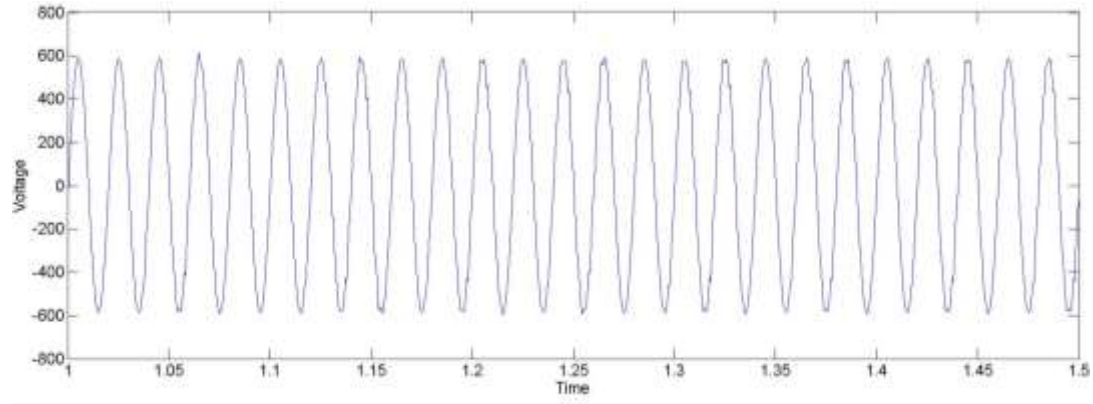

Figure 5.6. Faculty of agriculture 1 transformer voltage

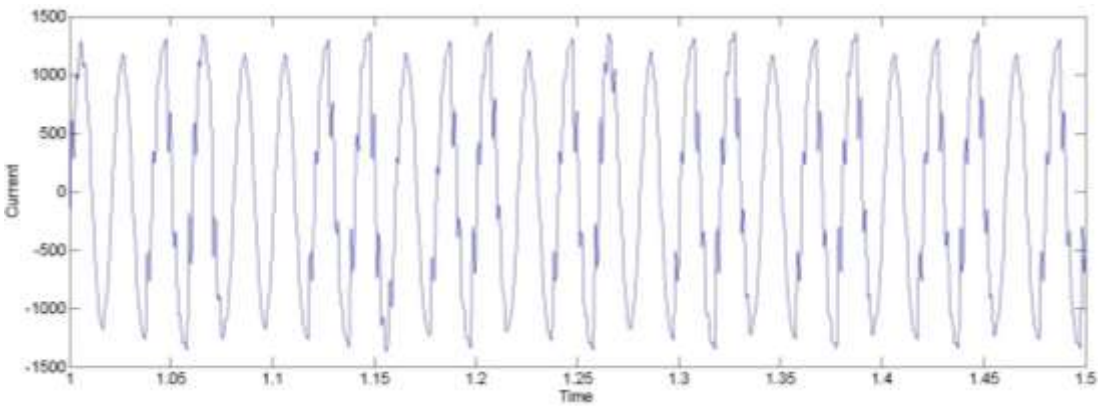

Figure 5.7. Faculty of agriculture 1 transformer current

As it can be seen from the figures above (Figure 5.2 - 5.7), even in case 5 which is the busiest case, installed infrastructure of Çukurova University can supply foreseen and studied electric vehicle charging infrastructure.

5.6. Total Harmonic Distortion (THD) Analysis

The summation of all harmonics in a system is known as total harmonic distortion (THD). THD, in mathematical terms, can also be defined as the root mean square (RMS) value of the total harmonics of the signal, divided by the RMS value of its fundamental signal.

The THD has a null value for a pure sinusoidal voltage or current. In our simulation (MatLab - Simulink) The THD block computes the total harmonic distortion (THD) of a periodic distorted signal. The signal can be measured as both voltage and current.

In thesis, case 5 is the busiest scenario among all scenarios. Thus, THD results of the case 5 are predicted to have the worst distortion values. THD values for both current and voltage are very small at the Main Supply, which are between 0.1-0.4% THD (Figure 5.8 and Figure 5.9). THD values for both current and voltage are very small at the Balcalı Hospital Transformer, which is between 0.1-0.6% THD (Figure 5.10 and Figure 5.11). THD values for voltage are very small at the Faculty of Agriculture 1 Transformer, which are between 0.1-0.15% THD (Figure 5.12), and for current are also small, which is between 4.5-4.55% THD (Figure 5.13).

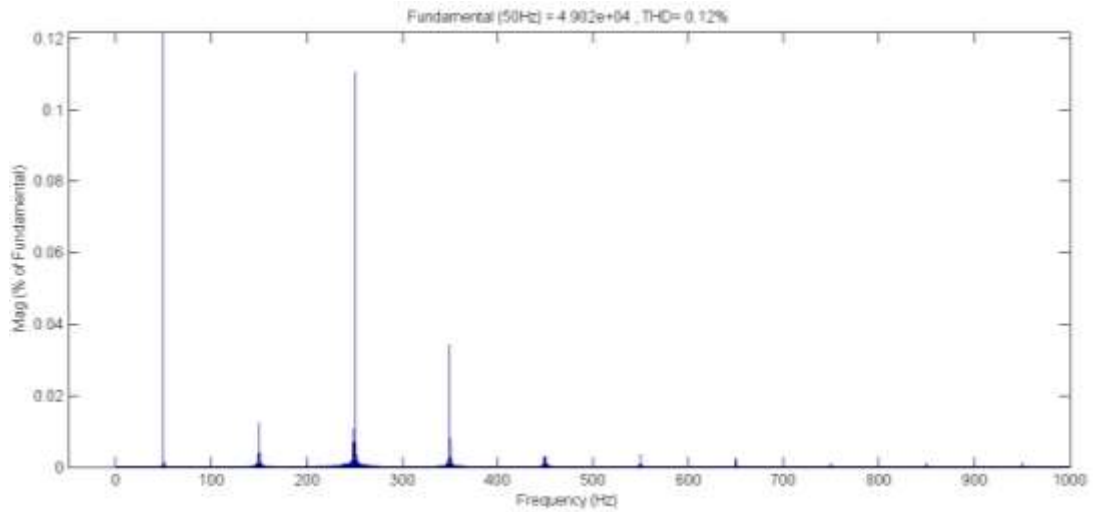

Figure 5.8. Main supply voltage THD

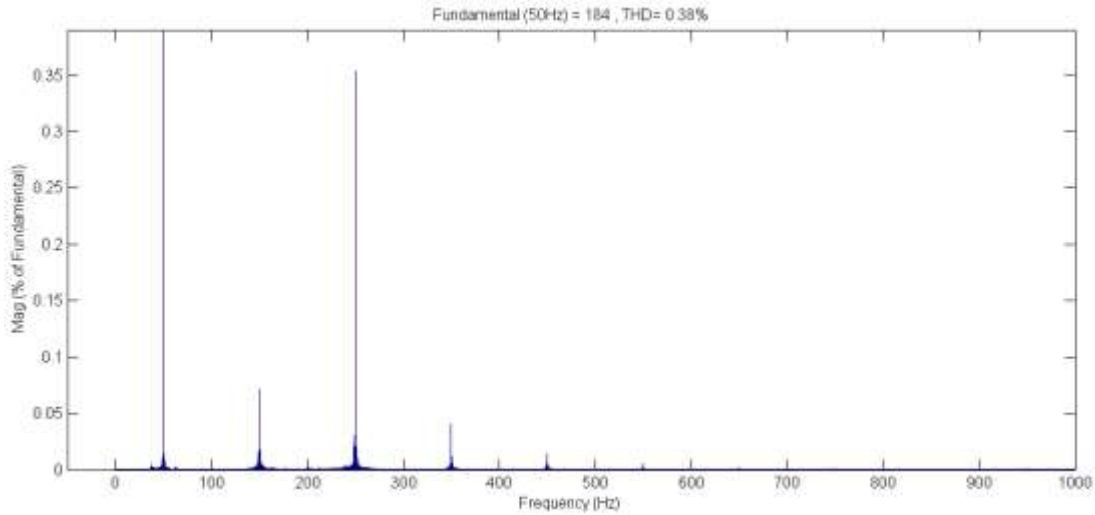

Figure 5.9. Main supply current THD

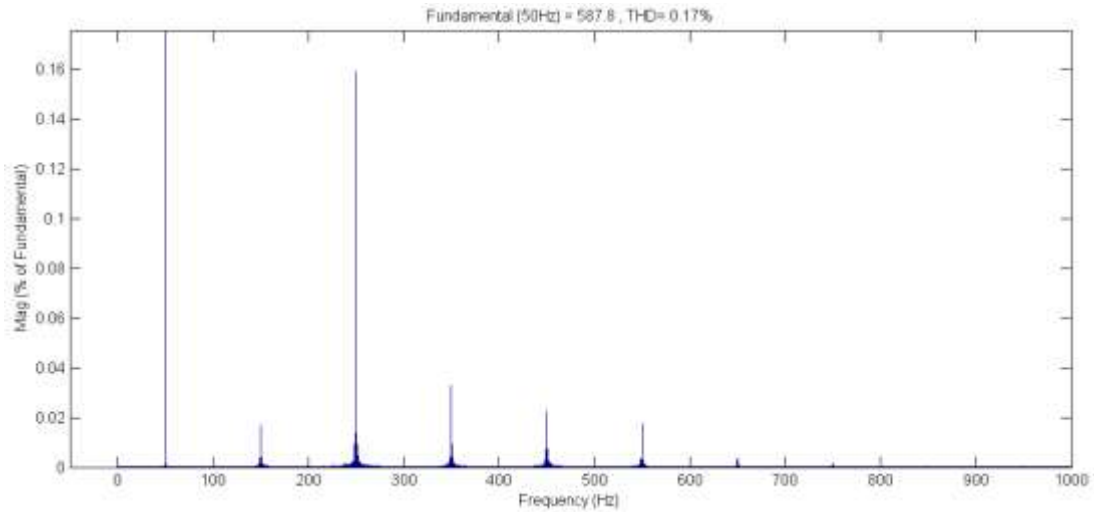

Figure 5.9. Balcalı hospital transformer voltage THD

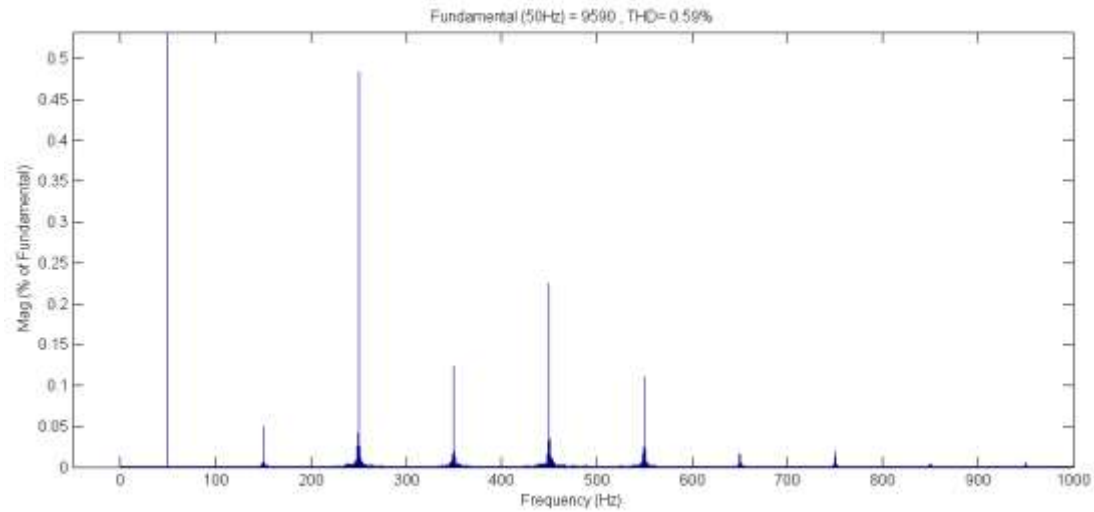

Figure 5.10. Balcalı hospital transformer current THD

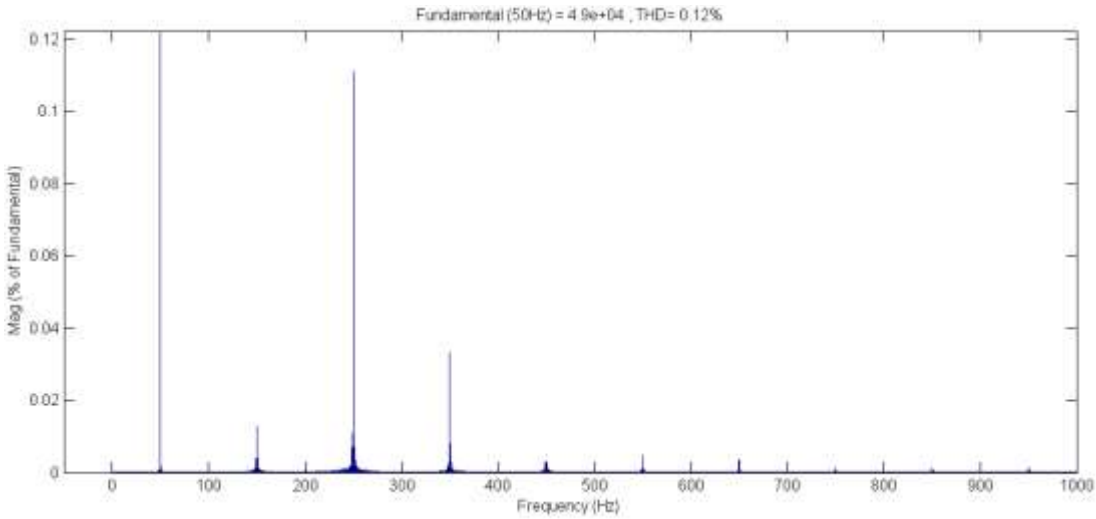

Figure 5.11. Faculty of agriculture 1 transformer voltage THD

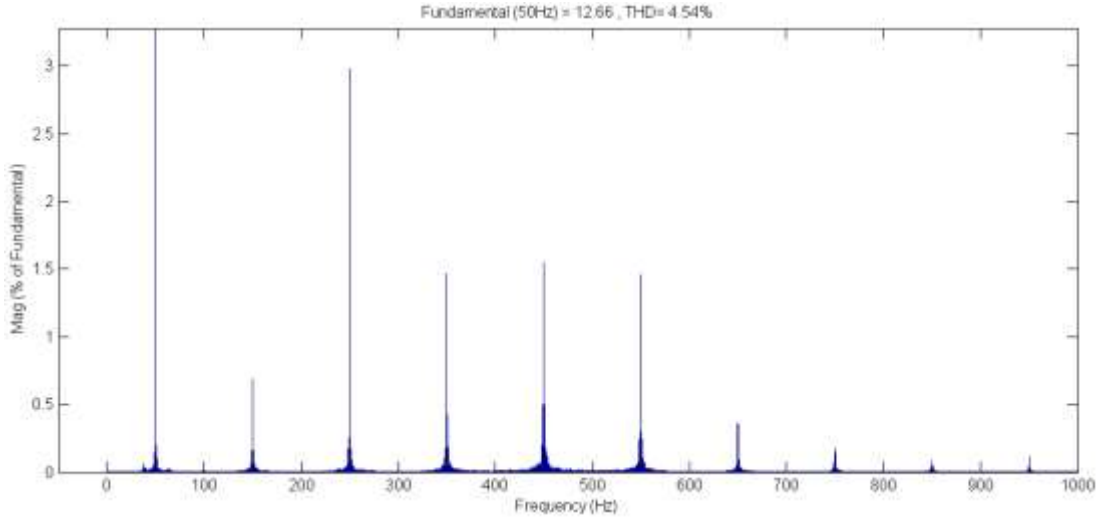

Figure 5.12. Faculty of agriculture 1 transformer current THD

For a standard HV system, authorized limitation of harmonic distortion must be under 5%. When the figures examined in detail, it is obviously seen that all THD values are fewer than 5%. Only Faculty of Agriculture 1 Transformer's current THD value has come close to the 5% limit. Because this transformer includes 4 charging blocks connected to it and these blocks recharging batteries simultaneously. Even so, studied system works under the limitations and could be used in the future electric vehicle infrastructure system.

6. CONCLUSION

Today, the demand for electric vehicles is increasing. Manufacturers have focused their research and development activities on the electric vehicles. The number of electric vehicles on the market is increasing day by the day. Therefore, the electric vehicle infrastructure technologies are also being developed. Some of the technology infrastructures are as follows: battery systems, communications, network integration, charging systems.

In this thesis, electric vehicle infrastructure technology in the charging systems and network integration issues are examined. Related modeling and simulation studies were performed in MatLab / Simulink. Also, battery charging topologies in the literature are discussed with their advantages and disadvantages. Their control systems are reviewed and the most appropriate one is chosen among them. This chosen controller system is constant current - constant voltage method. The main feature and the best advantage of this controller method are recharging the battery in the most appropriate and the most optimum manner. Battery charging systems and integration of the charging stations to the grid are one of the most important building blocks of electric vehicles' simulation, which will be applied in the university, is studied. Thus, this thesis is a basic exemplary study for electric vehicle charging stations which intended to be installed in the future in Çukurova University.

Upon reviewing the results of the studied system's current, voltage and active-reactive power values they were found to be suitable values. Harmonic values of the studied system's transformers which is given in the previous chapter, are below 5% that are also admissible. Thus, it can be easily said that the charger circuit was very successful during modeling simulations and additionally, results of the simulations have proved that Çukurova University's installed infrastructure has enough capacity to supply foreseen electric vehicle infrastructure. In the thesis, detailed modeling of charging circuits are developed and presented. Up to four charging circuits per 1kVA transformer are simulated. Furthermore, it's seen that up to seven charging circuits per 1kVA transformer can be built in order to develop a

bigger infrastructure to supply more crowded electric vehicle fleets and lastly, THD values of this setup are admissible.

Further research of this thesis could be carried out in the following areas:

- Performance evaluations of the different type of switching circuits for charging stations,
- Trial of different type of control methods for multitasking charging stations,
- Optimization of electric vehicle fleets integration to the charging stations,
- Integration of charging stations to smart grid system.

REFERENCES

AGGELER, D., CANALES, F., ZELAYA, H., PARRA, D.L., COCCIA, A., BUTCHER, N., APELDOOM, O., 2010. Ultra-Fast DC-Charge Infrastructures for EV-Mobility and Future Smart Grids. Innovative Smart Grid Technologies Conference, Pages: 1-8.

ANDERSON, P.M., FOUAD, A.A., 2003, Power System Control and Stability Second Edition. Wiley-IEEE Press

ARANCIBIA, A., STRUNZ, K., 2012. Modeling of an Electric Vehicle Charging Station for Fast DC Charging. IEEE International Electric Vehicle Conference, Pages: 1-6.

BUSO, S., MATTAVELLI, P., 2006. Digital Control in Power Electronics. Morgan and Claypool Publishers. 158 Pages.

CHEN, Y., PARRA, H.Z.D.L., HESS, F., 2012. Dynamic Simulation of EV Fast Charging with Integration of Renewables. IEEE International Conferences on Electric Vehicle Conference, Pages: 1-5.

DRIELS, M., 1996, Linear Control Systems Engineering, McGraw-Hill, New York, 625 p

DUBEY, A., SANTOSO, S., CLOUD, M.P., 2013. Average-Value Model of Electric Vehicle Chargers. IEEE Transactions on Smart Grid, Vol. 4, No. 3.

ERB, D.C., ONAR, O.C., KHALIGH, A., 2010. Bi-Directional Charging Topologies for Plug-In Hybrid Electric Vehicles. Applied Power Electronics Conference and Exposition (APEC), Pages: 2066 – 2072.

FEWSON, D., 1998. Introduction to Power Electronics. Butterworth-Heinemann; 1 edition. 208 Pages.

FIGUEIREDO, J.P.M., TOFOLI, F.L., SILVA, B.L.A., 2010. A review of singlephase PFC topologies based on the boost converter. in Proc. IEEE Int. Conf. Ind. Appl., Sao Paulo, Brazil, Nov., pp. 1–6.

FREIGE, M.D., ROSS, M., JOOS, G., DUBOIS, M., 2011. Power & Energy Ratings Optimization in a Fast-Charging Station for PHEV Batteries. IEEE International Electric Machines & Drives Conference, Pages: 486-489.

GAUTAM, D., MUSAVI, F., EDINGTON, M., EBERLE, W., DUNFORD, W.G., 2011. An automotive on-board 3.3 kW battery charger for PHEV application. in Proc. IEEE Veh. Power Propul. Conf., Chicago, IL, USA, Sep., pp. 1–6.

GAUTAM, D.S., MUSAVI, F., EDDINGTON, M., EBERLE, W., DUNFORD, W.G., 2012. An automotive on-board 3.3-kW battery charger for PHEV application. IEEE Trans. Veh. Technol., vol. 61, no. 8, pp. 3466–3474.

KISACIKOGLU, M.C., OZPINECI, B., TOLBERT, M., 2013. EV/PHEV Bidirectional Charger Assessment for V2G Reactive Power Operation. IEEE Transactions on Power Electronics, Vol. 28, No. 12.

KULARATNA, N., 1998. Power Electronics Design Handbook Low Power Components and Applications. Newnes; 1 edition. 300 Pages.

KUPERMAN, A., LEVY, U., GOREN, J., ZAFRANSKY, A., SAVERNIN, A., 2013. Battery Charger for Electric Vehicle Traction Battery Switch Station. IEEE Transactions On Industrial Electronics , Vol. 60, No. 12.

LIM, J.-W., KWON, B.-H., 1999. A power factor controller for single-phase PWM rectifiers. IEEE Trans. Ind. Electron., vol. 46, no. 5, pp. 1035–1037.

LUO, F.L., YE, H., Rashid, M., 2005. Digital Power Electronics and Applications. Academic Press; 1 edition. 464 Pages.

MACHIELS, N., LEEMPUT, N., GETH, F., ROY, J.V., BUSCHER, J., DRIESEN, J., 2014. Design Criteria for Electric Vehicles Fast Charge Infrastructure Based on Flemish Mobility Behaviour. IEEE Transactions on Smart Grid, Vol. 5, No. 1.

MAPELLI, F.L., TARSITANO, D., ANNESE, D., SALA, M., BOSIA, G., 2013. A Study of Urban Electric Bus with a Fast Charging Energy Storage System Based on Lithium Battery and Supercapacitors. International Conference and Exhibition on Ecological Vehicles and Renewable Energies, Pages: 1-9.

MARTINEZ, R., ENJETI, P.N., 1996. A high-performance single-phase rectifier with input power factor correction. IEEE Trans. Power Electron., vol. 11, no. 2, pp. 311–317.

MUSAVI, F., EDINGTON, M., EBERLE, W., DUNFORD, W.G., 2011. Energy efficiency in plug-in hybrid electric vehicle chargers: evaluation and comparison of front end ac-dc topologies. in Proc. IEEE Energy Convers. Congr. Expo., Phoenix, AZ, USA, Sep., pp. 273–280.

PILLAI, J.R., HUANG, S., THOGERSEN, P., MOLLER, J., BAK-JENSEN, B., 2012. Electric Vehicles in Low Voltage Residential Grid: A Danish Case Study. International Conference and Exhibition on Innovative Smart Grid Technologies, Pages: 1-7.

QIAN, H., ZHANG, J., LAI, J.-S., YU, W., 2011. A high-efficiency grid-tie battery energy storage system. IEEE Trans. Power Electron., vol. 26, no. 3, pp. 886–896.

RASHID M.H., 2014. Power Electronics: Devices, Circuits, and Applications Fourth Edition. PearsonEducation Inc., New Jersey.

STANLEY, G.R., BRADSHAW, K.M., 1999. Precision dc-to-ac power conversion by optimization of the output current waveform-the half bridge revisited. IEEE Trans. Power Electron., vol. 14, no. 2, pp. 372–380.

SUEKER, K.H., 2005. Power Electronics Design: A Practitoner's Guide. Newnes; 1 edition. 272 Pages.

TU, Y., LI, C., CHENG, L., LE, L., 2011. Research on Vehicle to Grid Techonology. International Conference on Computer Distributed Control and Intelligent Environmental Monitoring, Pages: 1013-1016.

VENERI, O., CAPASSO, C., FERRARO, L., DEL PIZZO, A., 2013. Performance Analysis on a Power Architecture for EV Ultra-Fast Charging Stations. Clean Electrical Power (ICCEP), 2013 International Conference, Pages: 183 – 188.

WILLIAMS, B.W., 1992. Power Electronics Devices, Driversi Applications, and Passive Components. Mcgraw-Hill. 560 Pages.

YILMAZ, M., KREIN, P.T., 2013. Review of Battery Charger Topologies, Charging Power Levels, and Infrastructure for Plug-In Electric and Hybrid Vehicles. IEEE Transactions on Power Electronics, Vol. 28, No. 5.

BIOGRAPHY

Adil Hakan CENGİZ was born in Adana, Turkey in 1988. He received his B.S. degree in Electrical and Electronics Engineering Department from Bahçeşehir University in 2009. After completion of his B.S. education, he started MSc education in Electrical and Electronics Engineering Department in Çukurova University. He has been working as a Research Assistant in Electrical and Electronics Engineering Department of the Çukurova University since 2012. His research areas are Electric Vehicles, Smart Grid and Power Electronics.